1 **Title:**

2 Physiological insight into the conserved properties of *Caenorhabditis elegans* acid-sensing

3 DEG/ENaCs

4

5 Eva Kaulich[1]*, Patrick T. N. McCubbin[1], William R. Schafer[1,2]*, Denise S. Walker[1]*

6

7 [1]Neurobiology Division, MRC Laboratory of Molecular Biology, Cambridge, UK.

8 [2]Department of Biology, KU Leuven, Leuven, Belgium.

9 *Corresponding authors. wschafer@mrc-lmb.cam.ac.uk, dwalker@mrc-lmb.cam.ac.uk,
10 ekaulich@mrc-lmb.cam.ac.uk

11

12

13 **Running title:** diversity in proton gating, and amiloride and zinc sensitivity

14

15 **Keywords:** Acid-sensing ion channel, degenerin/epithelial sodium channel, proton-gated, zinc,

16 amiloride

17

18 **Abstract:**

19 Acid sensing ion channels (ASICs) are members of the diverse family of degenerin/epithelial

20 sodium channels (DEG/ENaCs). They perform a wide range of physiological roles in healthy

21 organisms, including in gut function and synaptic transmission, but also play important roles

22 in disease, as acidosis is a hallmark of painful inflammatory and ischaemic conditions. We

23 performed a screen for acid-sensitivity on all 30 subunits of the *C. elegans* DEG/ENaC family

24 using Two-Electrode Voltage Clamp (TEVC) in *Xenopus* oocytes. We found two groups of acid-

25 sensing DEG/ENaCs characterised by being inhibited or activated by increasing proton

26 concentrations. Three of these acid-sensitive *C. elegans* DEG/ENaCs were activated by acidic

27 pH, making them functionally similar to the vertebrate ASICs. We also identified four new

28 members of the acid-inhibited DEG/ENaC group, giving a total of seven additional acid-

29 sensitive channels. We observed sensitivity to the anti-hypertensive drug amiloride as well as

30 modulation by the trace element zinc. Acid-sensitive DEG/ENaCs were found to be expressed

31 in both neurons and non-neuronal tissue, highlighting the likely functional diversity of these

32 channels. Our findings provide a framework to exploit the *C. elegans* channels as models to

33 study the function of these acid-sensing channels *in vivo,* as well as to study them as potential

34 targets for anti-helminthic drugs.

Introduction

35 Acidosis can occur under healthy physiological conditions, such as during synaptic

36 transmission (Du *et al.*, 2014), as well as being a hallmark of a wide range of pathologies. Cells

37 monitor tissue acidosis through membrane proteins including acid-sensing ion channels

38 (ASICs) (Vina *et al.*, 2013; Ortega-Ramirez *et al.*, 2017). ASICs belong to the conserved family

39 of Degenerin/Epithelial Sodium Channels (DEG/ENaC), non-voltage gated cation channels

40 that are involved in a diverse range of cellular processes. As the name indicates, the family

41 also includes mammalian ENaCs and *C. elegans* degenerins, as well as *Drosophila* pickpockets

42 (PPK) and an array of representatives from across animal phyla. Electrophysiological

43 approaches, particularly using *Xenopus* oocytes, have played an essential role in establishing

44 the physiology of channel properties of this diverse family (Canessa *et al.*, 1993; O'Brodovich

45 *et al.*, 1993; Canessa *et al.*, 1994; Schild *et al.*, 1997; Zhang & Canessa, 2002; Li *et al.*, 2009).

47 Acid-sensing DEG/ENaC members across species can be classified into two groups,

48 those activated and those inhibited by high proton concentrations. The former group includes

49 the mammalian ASICs (Waldmann *et al.*, 1997; Zhang & Canessa, 2002), zebrafish zASICs

50 (Chen *et al.*, 2007), human ENaCs (Collier & Snyder, 2009) and *Drosophila* PPK1 (Boiko *et al.*,

51 2012). Vertebrate ASICs are closed at neutral pH and generate proton-activated inward

52 currents, which increase with decreasing extracellular pH. However, the precise properties

53 depend on the subunit composition, with the half activation pH varying from around 6.5 to

54 4.5 (Waldmann *et al.*, 1997; Zhang & Canessa, 2002; Chen *et al.*, 2007). Together they thus

55 cover a significant pH range, with relevance to a diverse array of biological processes and

56 contexts. Heteromeric human αβγENaC channels, on the other hand, are open at neutral pH

57 with a maximal current at pH 6 and minimal current at pH 8.5 (Collier & Snyder, 2009),

58 correlating well with the pH range in the collecting duct of the kidney and other epithelia

59 where ENaCs are expressed. Rat αβγENaC currents are not altered over the same pH range,

60 highlighting variation between species (Collier & Snyder, 2009). The second group of proton-

61 sensitive DEG/ENaC members display inward currents at neutral pH, in the absence of

62 additional stimulus, and are blocked by acidic pH. This group consisted of only three members,

63 mouse ASIC5 (also called brain liver intestine Na$^+$ channel (BLINaC)) (Wiemuth & Grunder,

64 2010), *Trichoplax* TadNaC6 (Elkhatib *et al.*, 2019) and *C. elegans* ACD-1 (Wang *et al.*, 2008;

65 Wang *et al.*, 2012), to which we have added two more *C. elegans* channels, ACD-5 and the

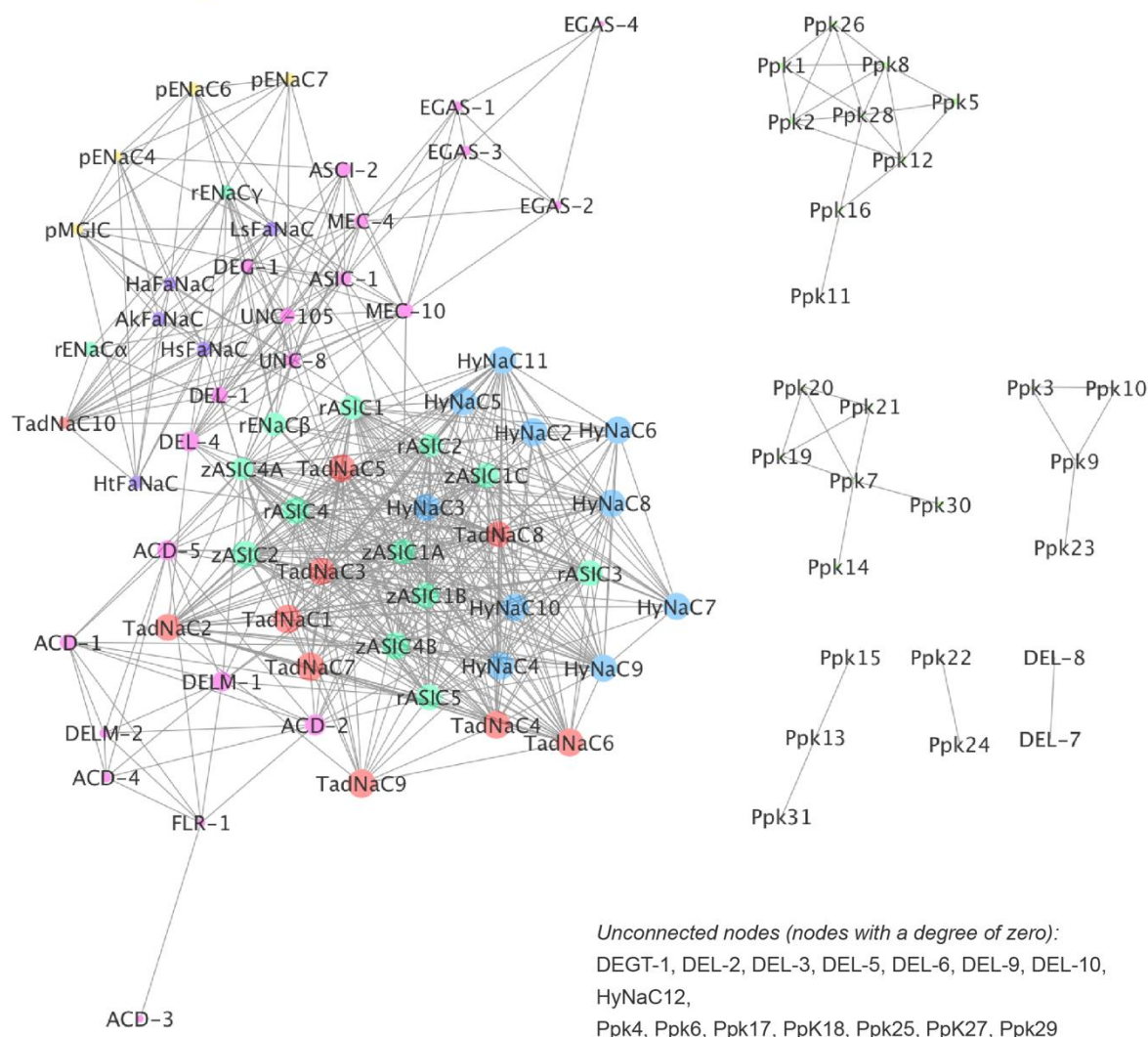66 heteromeric FLR-1/ACD-3/DEL-5 channel (Kaulich *et al.*, 2021).

67   The evidence linking ASICs to important roles in neuronal health and disease makes

68   them of particular interest, and tractable genetic model systems like *C. elegans* can facilitate

69   insights into these processes. For instance, gain-of-function mutations in the *C. elegans* DEG-

70   1, MEC-4 and UNC-8 subunits cause neuronal degeneration (Chalfie & Sulston, 1981; Bianchi

71   *et al.*, 2004; Wang *et al.*, 2013). Introducing one of the causative mutations into human ASIC2

72   also causes neuronal cell death, suggesting that ASIC2 might also be involved in

73   neurodegeneration (Waldmann *et al.*, 1996). This hypothesis has received attention since

74   ASIC2 is upregulated in patients with Multiple Sclerosis (MS), an inflammatory

75   neurodegenerative disease and pharmacological blocking of ASICs can lessen clinical

76   symptoms of inflammation and neuronal degeneration (Friese *et al.*, 2007; Fazia *et al.*, 2019).

77   ASICs (and *C. elegans* DEG/ENaCs) are also targets of diverse non-steroidal anti-inflammatory

78   drugs (NSAIDs) (Voilley *et al.*, 2001; Voilley, 2004; Fechner *et al.*, 2021), highlighting their

79   importance as targets for treating pain and inflammation (Dulai *et al.*, 2021). Finally, ASICs

80   could offer potential as targets for anti-helminthic drugs. A variety of compounds is currently

81   used to treat or prevent parasitic nematode infections, including imidazothiazoles and

82   macrocyclic lactones, which target nicotinic acetylcholine receptors and glutamate-gated

83   chloride channels, respectively (Wolstenholme & Rogers, 2005; Keiser & Utzinger, 2008;

84   Williamson *et al.*, 2009). Widespread resistance is a critical threat to both agriculture and

85   human health, so effective alternatives are urgently needed.

86   *C. elegans* DEG/ENaCs are vastly expanded compared to their vertebrate members,

87   with 30 subunit-encoding genes (compared to 4-5 in vertebrates). As the phylogram and the

88   Sequence Similarity Network (SSN) in Figure 1 and Figure 2 show, they form distinct homology

89   groups, with the vertebrate ENaCs and ASICs clustering separately. However, it is not clear

90   whether these clusters share functional characteristics. Indeed, the *C. elegans* DEG/ENaCs are

91   the only group with members in multiple clusters. The vertebrate ASICs closely cluster with

92   the TadNaCs from *Trichoplax adhaerens,* a primitive multicellular animal lacking any internal

93   organs and neurons, and both groups have members that are sensitive to changes in proton

94   concentration (Zhang & Canessa, 2002; Elkhatib *et al.*, 2019).

95   Despite the expansion and known diversity of *C. elegans* DEG/ENaCs, many members

96   lack functional characterization at the level of the channel, an obvious limitation when

97   interpreting their *in vivo* function. Therefore, we set out to perform a comprehensive screen

98   for acid-sensitive *C. elegans* DEG/ENaC channel subunits. In addition to five subunits that form

4

99 acid-inhibited homomers, we identified three acid-activated members. We demonstrate a

100 diversity in the effect of amiloride, with some being blocked, but others being unaffected or

101 potentiated, and also show that the acid-activated members exhibit diversity in ion selectivity.

102 Like their mammalian counterparts, their currents are blocked or potentiated by zinc,

103 indicating further conservation of function across phyla. This characterisation serves as a

104 starting point for further screens for compounds that affect these channels and for

105 understanding the molecular basis of diversity in DEG/ENaC function.

106

107

108 *Figure 1: Phylogram of the DEG/ENaC family.*
109 Polar view of a phylogenetic tree of the DEG/ENaC super-family, aligned in MAFFT version 7 (see
110 Methods for details). Tree scale represents the amount of genetic change. The data used to build these
111 networks originate from the UniProt Consortium databases and the InterPro and ENA databases from
112 EMBL-EBI. Colouring is according to phyla, as indicated. Accession numbers can be found in the
113 Supplementary table 1.

114

Figure 2: *Sequence Similarity Network (SSN) of the DEG/ENaC family.*

Sequence Similarity Network (SSN) of diverse members of the DEG/ENaC family. Generated using the web tool for SSNs for protein families (EFI-EST) developed by the Enzyme Function Initiative efi.igb.illinois.edu/ (Gerlt *et al.*, 2015; Gerlt, 2017; Zallot *et al.*, 2018; Zallot *et al.*, 2019). Each symbol represents a protein (node), two nodes are connected by a line (edge) if they share >25% sequence similarity and lengths of edges correlate with the relative dissimilarities of each pair. Relative positioning of disconnected clusters and nodes has no meaning. Unconnected notes, i.e. nodes with a degree of zero, are indicated on the bottom right-hand side. Cytoscape (Shannon *et al.*, 2003) is used to explore SSNs. Node sizes are determined by the degree of connectivity of the nodes (number of edges). The EFI-EST webtools use NCBI BLAST and CD-HIT to create SSNs. The computationally-guided functional profiling tool uses the CGFP programs from the Balskus Lab (https://www.microbialchemist.com/metagenomic-profiling/) (Levin *et al.*, 2017) and ShortBRED from the Huttenhower Lab (http://huttenhower.sph.harvard.edu/shortbred) (Kaminski *et al.*, 2015). The data used to build these networks originate from the UniProt Consortium databases and the InterPro and ENA databases from EMBL-EBI. Node colouring is according to phyla, as indicated. Accession numbers can be found in the Supplementary table 1.

6

132

133   **Methods**

134   **Protein sequences and alignment.**

135   Sequences of the DEG/ENaC superfamily were from UniProt, NBCI, Wormbase and Flybase,

136   combined into one file using SnapGene (Insightful Science, snapgene.com). Due to the recent

137   finding that removal of noisy or uncertain columns does not necessarily improve phylogenetic

138   reconstruction (Tan *et al.*, 2015), the complete amino acid sequences of the longest isoform

139   (where applicable) were used for the phylogenetic estimation of protein similarity. To address

140   the issue that variable regions tend to be over-aligned, and consequently, might lead to biases,

141   the robust aligners PRANK ((Loytynoja & Goldman, 2010) data not shown) and MAFFT (Katoh

142   *et al.*, 2002; Katoh & Standley, 2013) were used and confidence in the individual alignment

143   columns was assessed using GUIDANCE2. Both alignments generated were similar. We used

144   MAFFT (Katoh *et al.*, 2002; Katoh & Standley, 2013) as it allows re-adjustment alignment to

145   reflect information from sequences aligned later (Larkin *et al.*, 2007).

146

147   *Phylogram*. Visualisation of the DEG/ENaC super-family, protein sequences were aligned in

148   MAFFT version 7 multiple alignment program using rough distance and average linkage

149   UPGMA (unweighted pair group method with arithmetic mean) and the tree was visualized

150   using iTOL (Ciccarelli *et al.*, 2006; Kuraku *et al.*, 2013; Letunic & Bork, 2019).

151

152   *Sequence Similarity Network (SSN).* SSNs were generated using the web tool for SSNs for

153   protein   families   (EFI-EST)   developed   by   the   Enzyme   Function   Initiative   (EFI;

154   efi.igb.illinois.edu/) (Gerlt *et al.*, 2015; Gerlt, 2017; Zallot *et al.*, 2018; Zallot *et al.*, 2019).

155   Cytoscape (Shannon *et al.*, 2003) was used to explore SSNs. The EFI-EST webtools use NCBI

156   BLAST and CD-HIT to generate SSNs. The computationally-guided functional profiling tool uses

157   the CGFP programs from the Balskus Lab (https://bitbucket.org/biobakery/cgfp/src) (Levin *et*

158   *al.*,   2017)   and   ShortBRED   from   the   Huttenhower   Lab

159   (http://huttenhower.sph.harvard.edu/shortbred) (Kaminski *et al.*, 2015). The data used in

160   these analyses originated from the UniProt Consortium databases and the InterPro and ENA

161   databases from EMBL-EBI.

162

163 ***Molecular Biology***

164 The transcriptional reporters for the *Pdel-9::GFP* and *Pacd-2::GFP* plasmids were a kind gift

165 from Professor Kyuhyung Kim's lab (Daegu Gyeongbuk Institute of Science & Technology

166 (DGIST), Korea) containing 3113 bp upstream of the *del-9* gene and 3004 bp *acd-2* promoter

167 (2526 bp upstream of the start codon of *acd-2* and including 478 bp fragment of the *acd-2*

168 gene). The *asic-1* promoter consisted of 3500 bp upstream of the start codon. All plasmids,

169 including the fluorophore-reporter-fusions and cloning of cDNA into KSM vector for *Xenopus*

170 oocyte expression, were assembled using NEBuilder® HiFi DNA Assembly Master Mix

171 (Catalogue # E2621L). *C. elegans* cDNA was obtained from growing N2 wild-type animals on

172 fifteen 6cm NGM plates until the food was diminished, and subsequently extracted and

173 purified using the TRIzol Direct-zol RNA Miniprep (Catalogue #R2051, Zymo Research). cDNA

174 was generated using the Invitrogen™ SuperScript™ III First-Strand Synthesis System

175 (Catalogue # 18080051). Primers were designed using SnapGene 5.0.4. (Hifi-Cloning of two

176 fragments) based on the cDNA gene sequence found on wormbase.org, and ordered from

177 Integrated DNA Technologies Inc (IDT) (Leuven Belgium) or Sigma-Aldrich (Merck Life Science

178 UK Limited, Dorset, UK). The cDNA inserts were sub-cloned into the KSM vector under the

179 control of the T7 promoter, with 5' and 3' untranslated regions (UTRs) of the *Xenopus* beta-

180 globin gene and a poly(A) tail. The forward primer *agatctggttaccactaaaccagcc* and reverse

181 primer *tgcaggaattcgatatcaagcttatcgatacc* were used to amplify the KSM vector. NEB T_m

182 Calculator was used to determine annealing temperatures.

183

184 ***Two-Electrode Voltage Clamp (TEVC) in Xenopus oocytes***

185 cRNA was synthesized using the mMessage mMachine T3 Transcription Kit (Ambion #

186 AM1348), purified with GeneJET RNA Cleanup and Concentration Micro Kit (Thermo Scientific

187 # K0841) and eluted in 15µL RNase free water. *Xenopus laevis* oocytes of at least 1mm in size

188 were obtained from EcoCyte Bioscience (Dortmund, Germany). They were de-folliculated by

189 collagenase treatment and maintained in standard 1XND96 solution (96mM NaCl, 2mM $MgCl_2$,

190 5mM HEPES, 2mM KCl, 1.8mM $CaCl_2$, pH7.4). Oocytes were injected with 25µL of cRNA

191 solution at a total concentration of approximately 500 ng/µL using the Roboinject

192 (MultiChannel Systems). Oocytes were kept at 16°C in 1XND96 prior to TEVC. TEVC was

193 performed 1-2 days post-injection at room temperature using the Roboocyte2 (MultiChannel

194 Systems). *Xenopus* oocytes were clamped at −60 mV, using ready-to-use Measuring Heads

195   from MultiChannel Systems filled with 1.0 M KCl and 1.5 M K-acetate. All channels were

196   tested using the Roboocyte2 (MultiChannel Systems). For all current-voltage steps (I-V)

197   experiments, measurements were obtained in each solution once a steady-state current was

198   achieved and the background leak current was subtracted.

199   As millimolar concentrations of Ca^{2+} and other divalent ions except Mg^{2+} can block

200   ASIC currents (Paukert *et al.*, 2004), Ca^{2+}-free buffers were used for substitution experiments

201   of monovalent cations, adapted from a previous protocol (Hardege *et al.*, 2015): 96mM XCl,

202   1mM $MgCl_2$, 5mM HEPES, pH adjusted to 7.4 with XOH, where X was Na^+, K^+ or Li^+,

203   respectively. The osmolarity was checked and confirmed to be within the error of 210 mosm

204   or adjusted with D-Glucose if necessary (Awayda & Subramanyam, 1998). For testing pH

205   sensitivity, 1x ND96 solutions was used; for solutions with a pH 5 or lower, MES was used

206   instead of HEPES and adjusted with HCl. Actual current I-V curves for each individual oocyte

207   were fitted to a linear regression line and the x intercept was compared between solutions to

208   calculate an average reversal potential (E_{rev}). Reversal potential shift (ΔE_{rev}) when shifting

209   from a NaCl to a KCl or LiCl solution was calculated for each individual oocyte. In order to test

210   the responses to pH, the channel-expressing *Xenopus* oocytes were perfused with 1XND96

211   (using HEPES for buffering pH above 5.5 and MES for pH below 5), pH was adjusted with HCl

212   and ranged from pH 7.4 (neutral pH of the ND96 solution) to pH 4. For the Zn^{2+} dose-responses,

213   a 1 M $ZnCl_2$ stock solution in water (Catalogue #229997, Sigma-Aldrich) was diluted to the

214   desired concentrations in ND96 buffer based on a previously established protocol (Chen *et*

215   *al.*, 2012). Zn^{2+} was applied at increasing concentrations in the range of 0.1 μM to 5 mM.

216   Baseline subtraction and drift correction for all dose-responses was applied in the

217   Roboocyte2+ software (MultiChannel Systems). For analysis, currents were normalized to

218   maximal currents (I/I_{max}) and best fitted with the Hill equation (Variable slope) in GraphPad

219   Prism version 9.0.2.

220

221   ***Confocal microscopy***

222   Worms were mounted on 3% agar pads (in M9 (3 g KH_2PO4, 6 g Na_2HPO_4, 5 g NaCl, 1M $MgSO_4$))

223   in a 3 μL drop of M9 containing 25 mM sodium azide (NaN_3, Sigma-Aldrich). Images were

224   acquired using a Leica TCS SP8 STED 3X confocal microscope at 63x, 40x or 20x resolution and

225   Z stacks were generated using Fiji (ImageJ) (Schneider et al., 2012).

226

227 *Availability of materials*

228 *C. elegans* strains and plasmids generated for the purpose of this study are available upon

229 request from *wschafer@mrc-lmb.cam.ac.uk*.

230

231 **Results**

232 *Identification of two groups of acid-sensitive C. elegans DEG/ENaCs*

233 In contrast to the mammalian ASICs, which are activated in response to a drop in pH, ACD-1,

234 the only *C. elegans* DEG/ENaC for which proton sensitivity had been characterised in *Xenopus*

235 oocytes, is open at neutral pH and inhibited by low pH (Wang *et al.*, 2008). To identify other

236 acid-sensing *C. elegans* DEG/ENaC members, we performed a systematic screen for pH-

237 sensitive subunits using Two-Electrode Voltage Clamp (TEVC) in *Xenopus* oocytes injected

238 with cRNA, for all 30 *C. elegans* DEG/ENaCs. For the initial screen, oocytes were perfused with

239 pH 7.4 and pH 4 solutions, and currents were recorded and quantified (Figure 3A-E). We did

240 not go below pH 4 for the screen as our control *Xenopus* oocytes injected with nuclease free

241 water started responding to solutions below pH 4. We identified two groups of acid-sensing

242 DEG/ENaCs. One group included the previously characterised ACD-1 (Wang *et al.*, 2008)

243 (Figure 3B), showing currents at neutral pH (pH 7.4) that were decreased at low pH (pH 4).

244 We identified four additional members, ACD-5, DEL-4 DELM-1 and UNC-105 (isoform h),

245 which also fit this profile and which we will refer to here as acid-inhibited channels (Figure

246 3D). Interestingly, we also found three members that showed robustly increased currents at

247 low pH, i.e. that were opened, or further opened, in response to increasing proton

248 concentrations; these were ASIC-1, ACD-2 and DEL-9 (Figure 3C). We designated the members

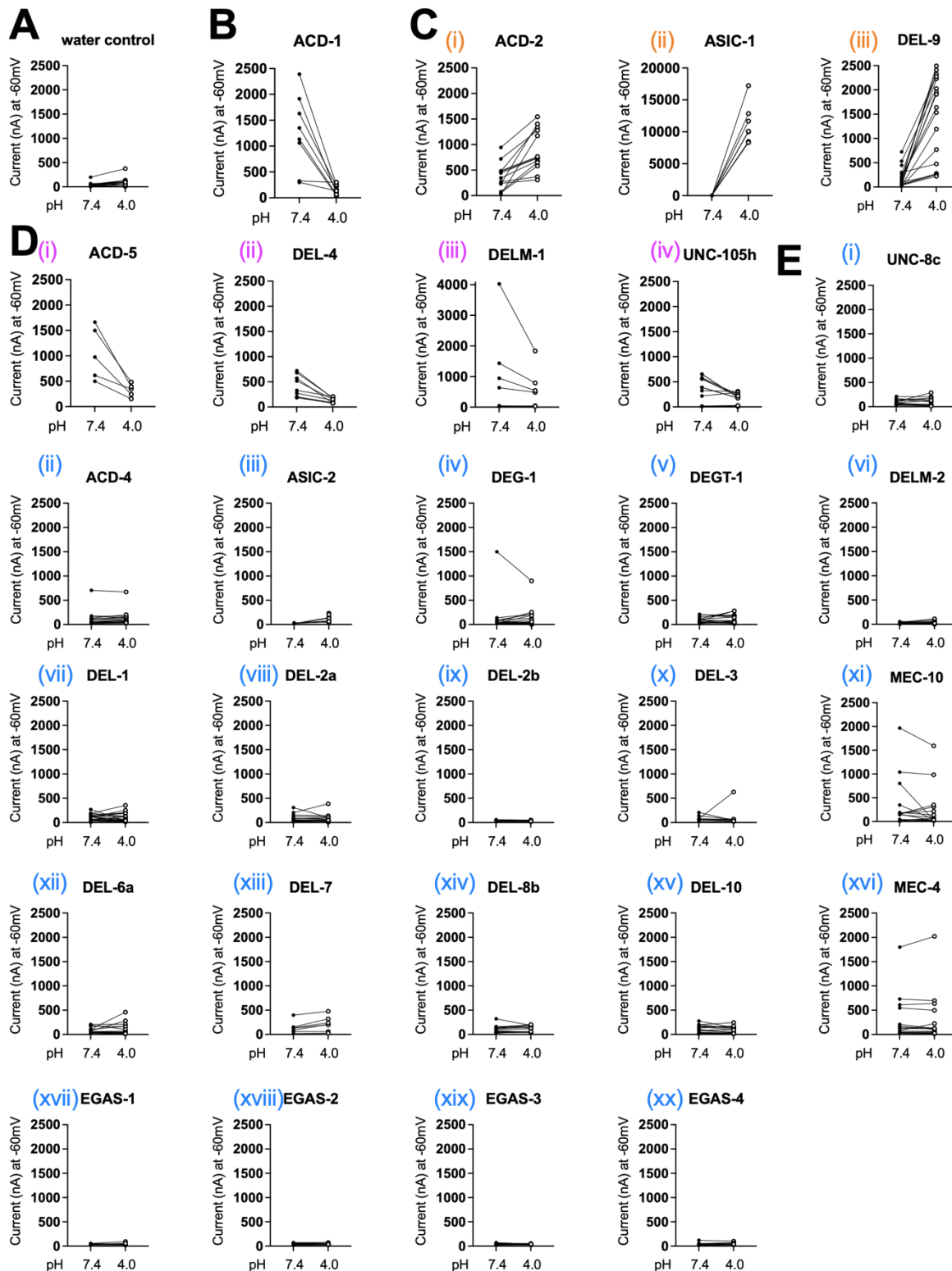249 in this second group as acid-activated channels.

250

Figure 3: *Quantification of current at pH 7.4 and pH 4 of Xenopus oocytes* expressing *C. elegans DEG/ENaC subunits.*

Xenopus oocytes injected with the respective cRNA. Lines connect data from individual oocytes. (A) Nuclease-free water injected oocytes serve as negative controls (n=13). (B) ACD-1 (n=8) expressing oocytes serve as a positive control (Wang *et al.*, 2008). (C) Constructs that form acid-activated channels: ACD-2 (n=13), ASIC-1 (n=7) and DEL-9 (n=19). (D) Constructs that form acid-inhibited channels: ACD-5 (n=5), DEL-4 (n=9), DELM-1 (n=7), UNC-105 (n=17). (E) *Xenopus* oocytes injected with

11

259　the respective cRNA do not display acid-sensitive currents: UNC-8c (n=14), ACD-4 (n=23), ASIC-2
260　(n=21), DEG-1 (n=23), DEGT-1 (n=23), DELM-2 (n=24), DEL-1 (n=24), DEL-2a (n=18), DEL-2b (n=10),
261　DEL-3 (n=10), MEC-10 (n=17), DEL-6a (n=23), DEL-7 (n=7), DEL-8b (n=20), DEL-10 (n=18), MEC-4 (n=16),
262　EGAS-1 (n=12), EGAS-2 (n=12), EGAS-3 (n=11), EGAS-4 (n=12). The pH-insensitive currents of ACD-3
263　and DEL-5 are published elsewhere (Kaulich *et al.*, 2021). Axis labels: y= actual current in nA; x =
264　perfusion with either pH 7.4 (closed circle) or pH 4 (open circle) as indicated. Holding potential was -
265　60mV. Experiments were repeated more than three times and on different days and were pooled
266　together. Note that all graphs are plotted using the same scale, except ASIC-1 and DELM-1, due to the
267　large currents observed in oocytes expressing these two constructs.
268

269　### *The C. elegans DEG/ENaCs include both acid-inhibited and acid-activated*
270　### *channels*

271　To characterise the acid-sensitivity and ion selectivity of the acid-sensitive DEG/ENaCs

272　identified in the screen, we perfused different pH solutions over the oocytes expressing the

273　respective cRNA and substituted different monovalent cations in the recording solution. The

274　ion selectivity experiments were performed at pH_{50} concentrations and the shift in reversal

275　potential (ΔE_{rev}) was assessed after substituting NaCl with either KCl or LiCl in the solution

276　containing 96mM NaCl, 1mM $MgCl_2$, 5mM MES, based on a previous protocol (Hardege et al.,

277　2015). The osmolarity was adjusted to 210 mosm using D-Glucose (Awayda & Subramanyam,

278　1998). All ion-substitution experiments were conducted in the absence of Ca^{2+} as Ca^{2+} has

279　been shown to be able to block ASIC channels (Paukert et al., 2004).

280　　　We first investigated the properties of the acid-inhibited channels. ACD-5, which we

281　have described elsewhere, was permeable to Li^+ and to a lesser degree to Na^+ and K^+ but

282　impermeable for Ca^{2+} and exhibited maximal current at approximately pH 6 and was inhibited

283　by both lower and higher pH, with pH_{50}s of 4.87 and 6.48 (Kaulich *et al.*, 2021). In contrast,

284　DEL-4 was shown to be a Na^+ channel that can be blocked in the range of pH 8-4 with pH_{50} of

285　5.7 (Petratou *et al.*, submitted). DELM-1 had previously been characterised as an amiloride-

286　sensitive channel permeable for Li^+ and Na^+, and to a lesser degree to K^+ (Han *et al.*, 2013).

287　We found that DELM-1 was inhibited by acidic pH with a pH_{50} of 5.75 (Figure 4A, B). The Na^+

288　and K^+ permeable UNC-105 has previously been implicated in proton-sensing *in vivo* in

289　muscles (Jospin & Allard, 2004). We found that UNC-105 (isoform h) produced small currents

290　which were inhibited when perfused with pH in the range of pH 9-4 with a pH_{50} of 6.42 (Figure

291　4A, B).

292　　　By contrast, for all three acid-activated subunits, acid-evoked currents increased in a

293　concentration-dependent manner. We observed an excitatory pH_{50} of 4.49 for ASIC-1, pH_{50}

294   of 5.03 for ACD-2 and pH_{50} of 4.27 for DEL-9. (Figure 5A, B). None of the three homomeric

295   channels desensitized, but reached a plateau after several seconds, with ASIC-1 and ACD-2

296   reaching the plateau much faster than DEL-9, as shown by the timescale in Figure 5A, B. This

297   is not an artefact of the perfusion rate as the same perfusion rate was used for all oocytes

298   and conditions. ACD-2 partially desensitised at pH 4 (and below, Supplementary figure S1),

299   which might be relevant to the channel's physiological pH range.

300   As no physiological data was available for any of the three acid-activated DEG/ENaC

301   subunits, we investigated their ion selectivity by carrying out ion substitution experiments.

302   Our results showed that ASIC-1 exhibits a preference of K^+ and Li^+ over Na^+, with a median

303   positive shift in E_{rev} of 12.2 mV, when shifting from a NaCl solution to a KCl or LiCl solution

304   (Figure 5C, D). In contrast ACD-2 was observed to be a sodium channel, selective for Li^+ and

305   Na^+ over K^+ with no change in E_{rev} when switching from a NaCl to a LiCl solution, but a large

306   median negative shift in E_{rev} of -43.3 mV when shifting from a NaCl solution to a KCl solution

307   (Figure 5C, D). This ion selectivity property is similar to that previously described for DELM-1

308   (Han *et al.*, 2013). Finally, DEL-9 was non-selective for monovalent cations, showing no shift

309   in reversal potential when switching between solutions (Figure 5C, D). Thus, the newly

310   characterised acid-sensitive DEG/ENaCs showed significant diversity in their ion selectivity

311   properties, consistent with previous findings on other family members (Canessa *et al.*, 1994;

312   Wang *et al.*, 2008; Carattino & Della Vecchia, 2012; Fechner *et al.*, 2021).
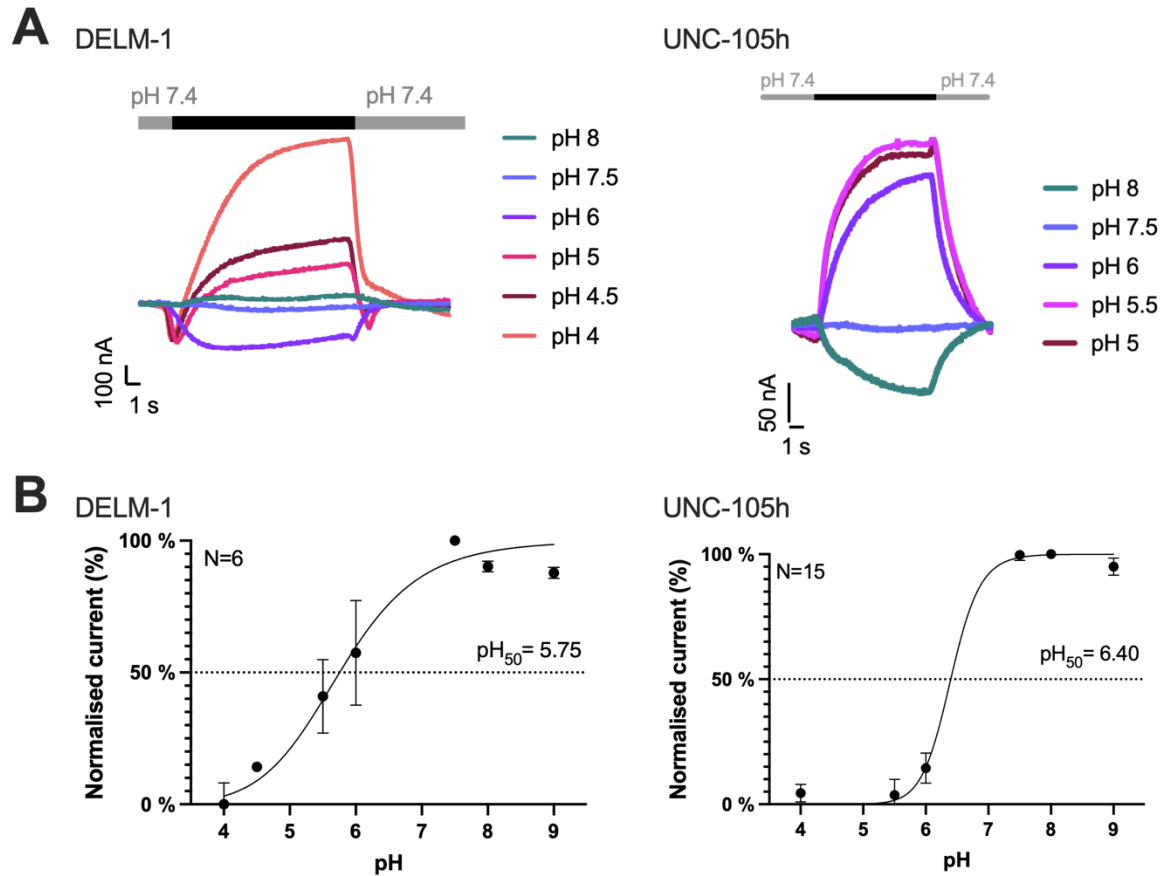
313

Figure 4: DELM-1 and UNC-105 form acid-inhibited homomeric channels.

(A) Representative traces of *Xenopus* oocytes expressing the respective construct when perfused with solutions of different pH, lowering of pH (black bar) from a holding pH of 7.4. (B) Current-pH relationship. Dotted line indicates pH_{50}. DELM-1, pH_{50} = 5.75 ± 0.23 (N = 6). UNC-105 isoform h, pH_{50} = 6.42 ± 0.10 (N = 15). Currents were recorded at a holding potential of – 60mV, normalized to maximal currents (I/I_{max}) and best fitted with the Hill equation (Variable slope). Error bars represent Mean ± SEM.
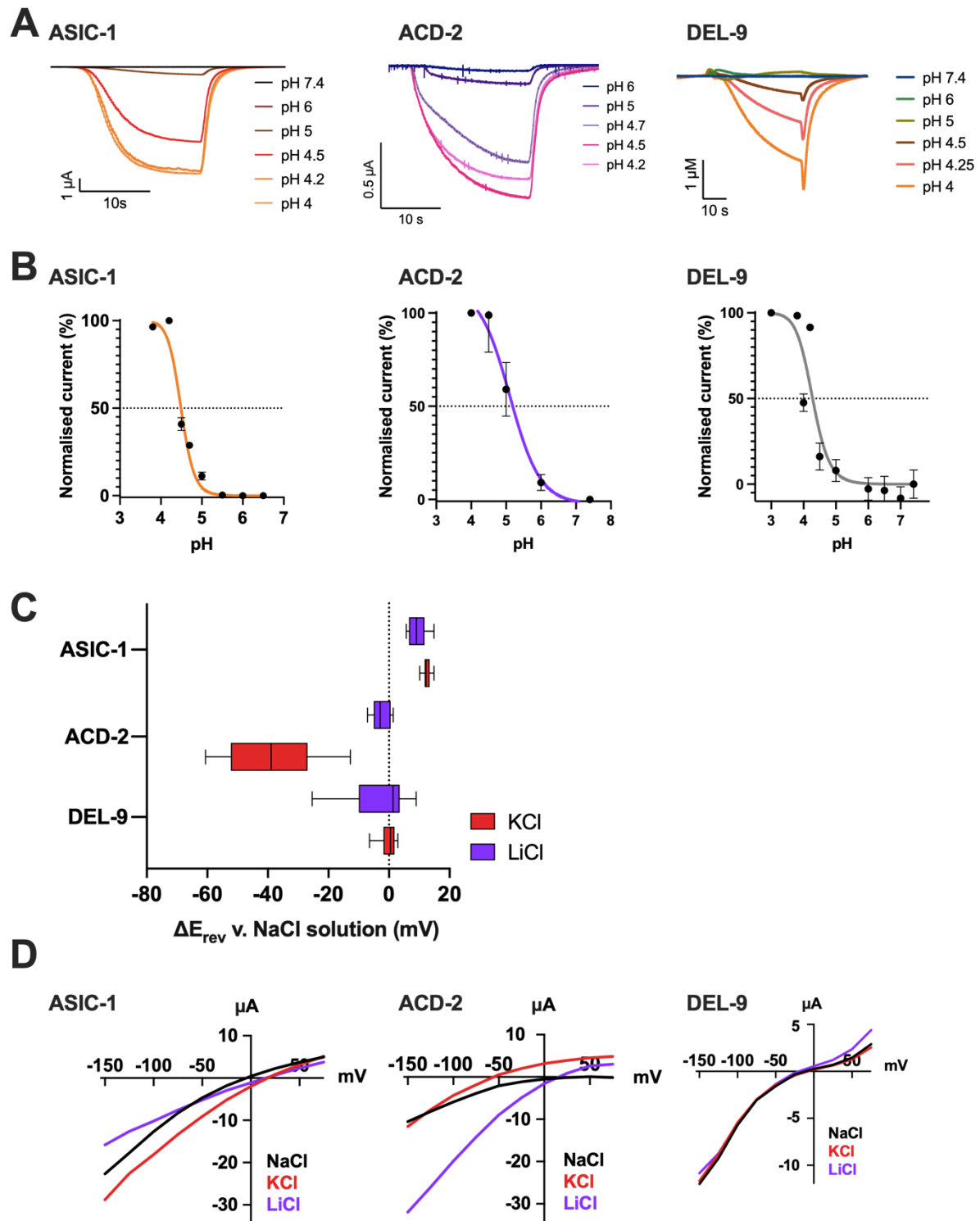
Figure 5: ASIC-1, ACD-2 and DEL-9 form acid-activated homomeric channels permeable for monomeric cations.

(A) Representative traces of *Xenopus* oocytes expressing the respective construct when perfused with solutions of different pH, lowering of pH from a holding pH of 7.4. (B) Current-pH relationship. Dotted line indicates pH_{50}. ASIC-1, pH_{50} = 4.49 ± 0.02 (N = 13). ACD-2, pH_{50} = 5.028 ± 0.109 (N = 6). DEL-9, pH_{50} = 4.27 ± 0.07 (N = 10). Currents were recorded at a holding potential of −60mV, normalized to maximal currents (I/I_{max}) and best fitted with the Hill equation (Variable slope). Error bars represent Mean ± SEM. (C-D) Summary of Ion selectivity. ASIC-1, ACD-2 and DEL-9 are permeable for monomeric cations.

15

332   (C) Average calculated from 4<N<12 oocytes for each construct of ΔE_{rev} when shifting from a NaCl
333   solution to KCl or LiCl solution. A negative shift of E_{rev} indicating a preference for Na^+ over the
334   respective ion and a positive shift indicating a preference of the respective ion over Na^+. Data is
335   presented as box-plots (hinges of the plot are the 25th to 75th percentiles) with Median and whiskers
336   of 1.5IQD (inter-quartile distance, as calculated by the Tukey method). (D) Representative current-
337   voltage (IV) relationships for oocytes expressing ASIC-1, ACD-2 and DEL-9. Actual current for each
338   oocyte and baseline current subtracted from acid-evoked current at pH_{50} concentrations (see panel B
339   for reference). The oocyte membrane was clamped at −60 mV and voltage steps from -150 mV to +75
340   mV were applied as indicated. Currents are actual currents in µA (y-axis), voltage steps in mV (x-axis)
341   as indicated. Error bars represent Mean ± SEM.
342

343   *Exploring the effect of known DEG/ENaC modulators amiloride and zinc*

344   Both amiloride and zinc can act as blockers for some DEG/EnaCs and as enhancers for others,

345   again showing the functional diversity of this channel family. Amiloride is an anti-hypertensive

346   drug, acting on the human ENaCs in the kidney (Teiwes & Toto, 2007; Bhagatwala *et al.*, 2014).

347   It is a potent blocker of many, but not all DEG/ENaCs. Previous work showed that homomeric

348   ASIC3, ASIC2 and heteromeric ASIC3/ASIC1b are potentiated by amiloride, whereas *C. elegans*

349   DEGT-1 is amiloride-insensitive (Bentley, 1968; Palmer & Frindt, 1986; Canessa *et al.*, 1994;

350   Schild *et al.*, 1997; Adams *et al.*, 1999; Kellenberger *et al.*, 2003; Li *et al.*, 2011; Baconguis *et

351   al.*, 2014; Besson *et al.*, 2017; Fechner *et al.*, 2021; Matasic *et al.*, 2021). Therefore, we

352   investigated if the acid-evoked currents at the respective pH_{50} of ASIC-1, ACD-2 and DEL-9

353   could be blocked by or potentiated by amiloride (Figure 6; for pH_{50} see Figure 5B for

354   reference). We observed that ASIC-1 and ACD-2 are sensitive to amiloride; indeed acid-

355   evoked currents could be blocked in a dose-dependent manner, which is also a common

356   characteristic of the DEG/ENaC super-family (Vullo & Kellenberger, 2020). Amiloride blocked

357   ASIC-1 acid-evoked currents with an IC_{50} of 134 µM (Figure 6B) and ACD-2 acid-evoked

358   currents with an IC_{50} of 84 µM (Figure 6C). By contrast, DEL-9 acid-activated currents were

359   insensitive to amiloride (Figure 6D).

360   We also investigated the effect of amiloride on the acid-inhibited subunits, ACD-1,

361   DELM-1 and UNC-105, ACD-5 and DEL-4. We observed that all were inhibited by amiloride

362   (Supplementary figure 2, see also (Jospin & Allard, 2004; Wang *et al.*, 2008; Han *et al.*, 2013;

363   Kaulich *et al.*, 2021) (Petratou *et al.*, submitted)). UNC-105 showed paradoxical block for

364   amiloride with an EC_{50} of 14.56 µM amiloride and a strong inhibition at 1 µM (Figure 7 A, B).

365   From the screen shown in Figure 3, we found other DEG/ENaC subunits exhibiting a

366   current at pH 7.4. This "leak" current at pH 7.4 could be an indicator of an open channel,

367 which may or may not be constitutively open in its physiological context, depending on the

368 pH range of its environment, or it might be independent of pH-sensitivity. However, a leak

369 current could also potentially result from non-functional channel expression making the

370 oocytes unhealthy. Since amiloride can have either a potentiating or inhibitory effect on the

371 channel's current, we also examined amiloride sensitivity for all other DEG/ENaC channels.

372 We found that whereas most channels' currents were unaffected by amiloride and the

373 currents at pH 7.4 persisted (Supplementary figures 3 and 4), DEL-5, DEL-8b and DEL-9

374 currents at pH 7.4 were significantly potentiated by amiloride (see also (Kaulich *et al.*, 2021))

375 (Supplementary figure 5). Thus, the effect of amiloride on channel activity varied widely

376 between different members of the *C. elegans* DEG/ENaC family.

377   Zinc is an essential trace element in the brain that is present in synaptic vesicles in a

378 subgroup of glutamatergic neurons and co-released with glutamate in response to high-

379 frequency stimulation (Assaf & Chung, 1984; Howell *et al.*, 1984; Frederickson & Moncrieff,

380 1994). High concentrations of Zn^{2+} potentiate acid-evoked currents of homomeric and

381 heteromeric ASIC2a-containing channels (Baron *et al.*, 2001). By contrast, Zn^{2+} can block

382 ASIC1b subunits, in which multiple binding sites for Zn^{2+} in the extracellular domain have been

383 proposed (Baron *et al.*, 2001; Jiang *et al.*, 2012). We therefore investigated the effect of Zn^{2+}

384 on the newly characterised acid-sensing channels. We found that the pH_{50}-evoked transient

385 currents of the acid-activated channels could be blocked by Zn^{2+} in a dose-dependent manner,

386 with an IC_{50} of 132.4 µM Zn^{2+} for ASIC-1, an IC_{50} of 46.39 µM Zn^{2+} for ACD-2, and an IC_{50} of

387 58.33 µM Zn^{2+} for DEL-9 (Figure 8). We further tested Zn^{2+} modulation at pH 7.4 (which

388 corresponds to the open state of the channels) of the acid-inhibited channels and found that

389 similar to the acid-activated channels, the acid-inhibited ACD-1, ACD-5, DEL-4 and UNC-105

390 were blocked by increasing concentrations of Zn^{2+} with IC_{50}s of 184.4 µM, 165 µM, 12.25 µM

391 and 31.94 µM, respectively (Figure 9A, B, D, E). In contrast, increasing concentrations of Zn^{2+}

392 potentiated the baseline currents of DELM-1 with an EC_{50} of 238.3 µM (Figure 9C). This

393 demonstrates that like their mammalian counterparts, those acid-sensing DEG/ENaCs can be

394 modulated by Zn^{2+} in an inhibiting or potentiating manner. This demonstrates that *C. elegans*

395 acid-sensing DEG/ENaCs share the function of zinc- and amiloride-modulation with their
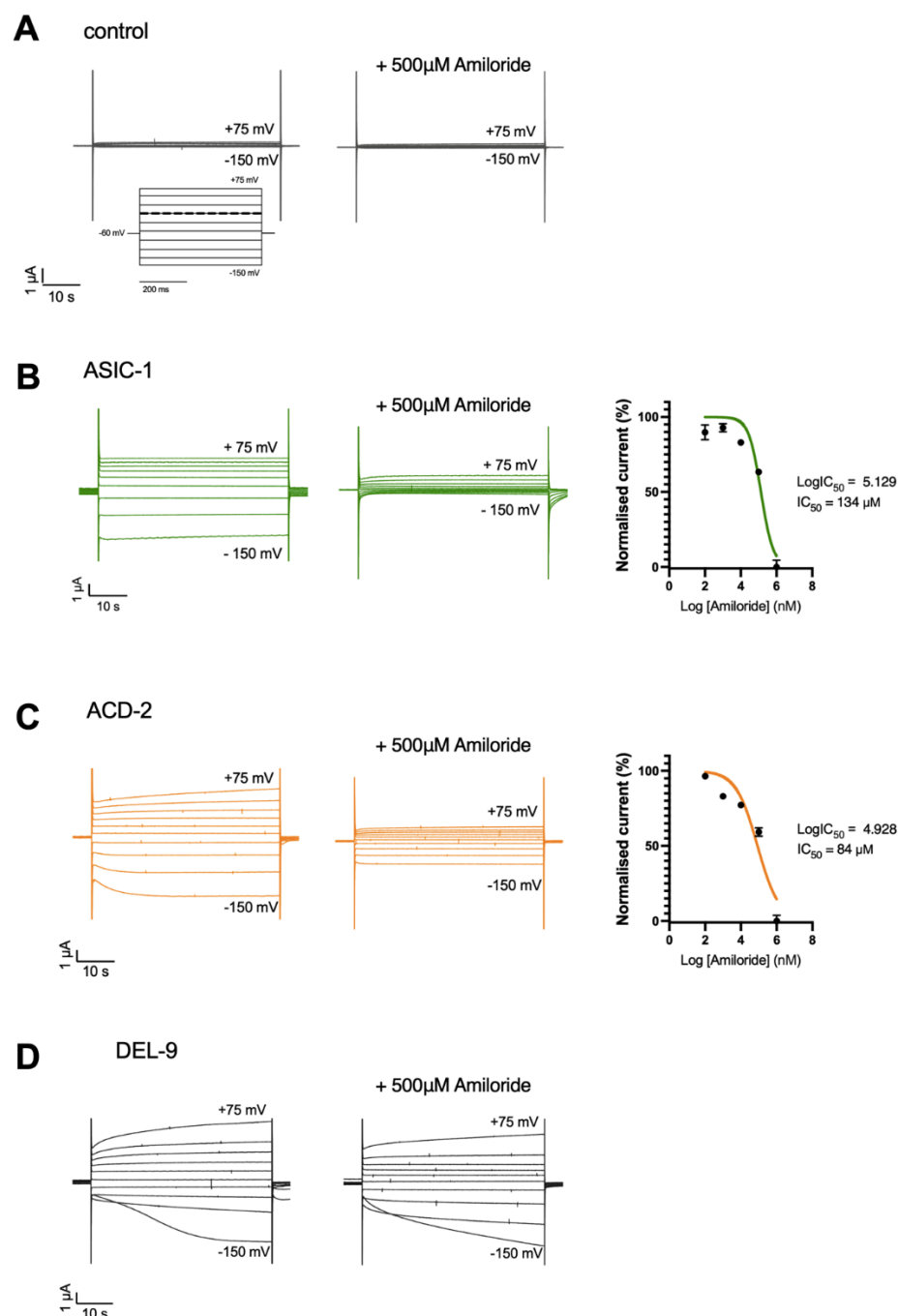
396 vertebrate homologues.

Figure 6: *Amiloride-sensitivity ACD-2, ASIC-1 and DEL-9.*
ASIC-1 and ACD-2 (but not DEL-9) acid-evoked transient currents can be blocked by amiloride. Representative acid-evoked transient currents in the absence (left) and presence of 500 µM amiloride (middle) at pH_{50} (for pH_{50} of each channel see Figure 5B). (A) Nuclease-free water-injected oocytes (negative control) are unaffected by low pH (example shown here pH 4.5) or amiloride. (B) Amiloride dose-response of ASIC-1 with an IC_{50} of 134 µM amiloride (N = 10) and (C) ACD-2 with an IC_{50} of 84 µM amiloride (N = 12). (D) DEL-9 (N=10) acid-activated transient currents are unaffected by amiloride. Currents were recorded at a holding potential of - 60mV and are normalised to the maximum current (I_{max}) calculated for each oocyte individually, and best fitted with the Hill equation (Variable slope). The *Xenopus* oocyte membrane was clamped at −60 mV and voltage steps from -150 mV to +75 mV were applied as indicated. Currents are actual currents in µA (y-axis), voltage steps in mV (x-axis) as indicated. Error bars represent Mean ± SEM.

18
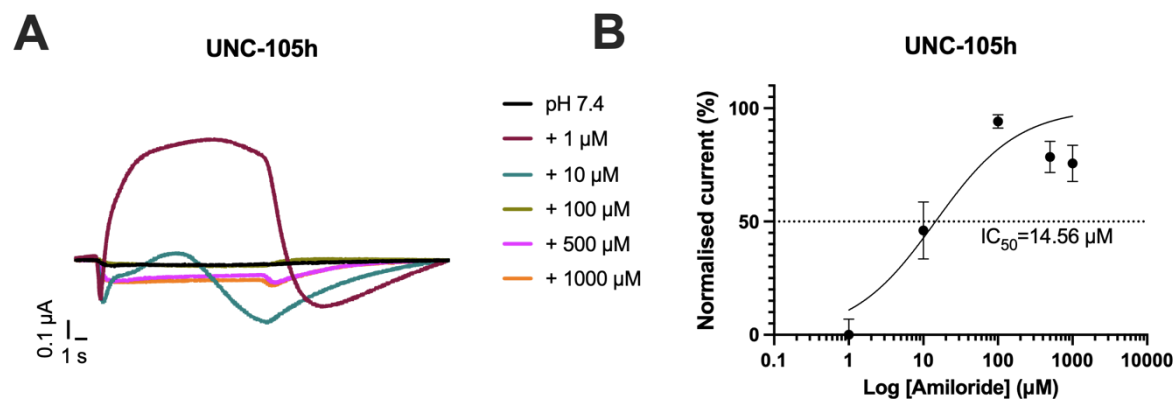
410

411

Figure 7: *Paradoxical effect of amiloride on UNC-105.*

UNC-105 (isoform h) transient currents at pH 7.4 can be blocked by amiloride. (A) Representative transient currents at increasing concentrations of amiloride. Amiloride blocks the channel at 1 µM concentration but other concentrations do not affect the currents. The *Xenopus* oocyte membrane was clamped at −60 mV. Currents are actual currents in µA (y-axis), voltage steps in mV (x-axis) as indicated. (B) Amiloride dose-response of UNC-105 with an EC_{50} of 14.56 µM amiloride (N = 16). Currents were recorded at a holding potential of - 60mV and are normalised to the maximum current (I_{max}) calculated for each oocyte individually, and best fitted with the Hill equation (Variable slope). Error bars represent Mean ± SEM.
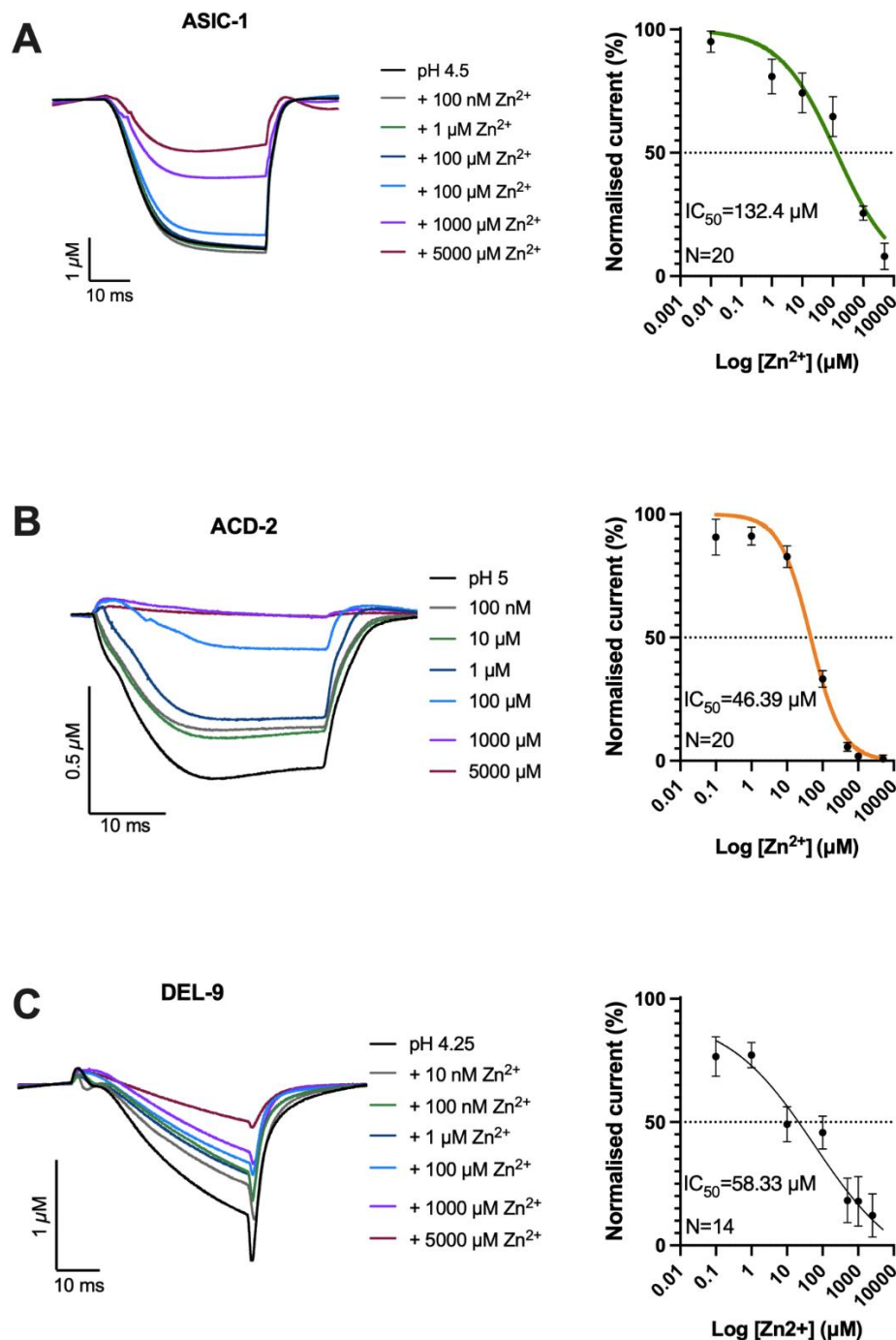
421

Figure 8: Zinc modulation of acid-activated DEG/ENaC channels in Xenopus oocytes.
Zn^{2+} can block homomeric ASIC-1, ACD-2 and DEL-9 acid-evoked currents. Shown are representative example traces (Left) and dose response curves (Right) for each channel. (A) ASCI-1 (N=20), (B) ACD-2 (N=20) and (C) DEL-9 (N=14) pH_{50}-evoked transient currents can be blocked by Zn^{2+} in a dose-dependent manner (at pH_{50} of each channel). Zn^{2+} dose-response of ASIC-1 with an IC_{50} of 132.4 µM Zn^{2+}, ACD-2 with an IC_{50} of 46.39 µM Zn^{2+} and DEL-9 with an IC_{50} of 58.33 µM Zn^{2+}. Baseline subtraction and drift correction was applied in the Roobocye2+ software. Currents were recorded at a holding potential of - 60mV and are normalised to the maximum current (I_{max}) calculated for each oocyte individually, and best fitted with the Hill equation (Variable slope). Error bars represent Mean ± SEM.
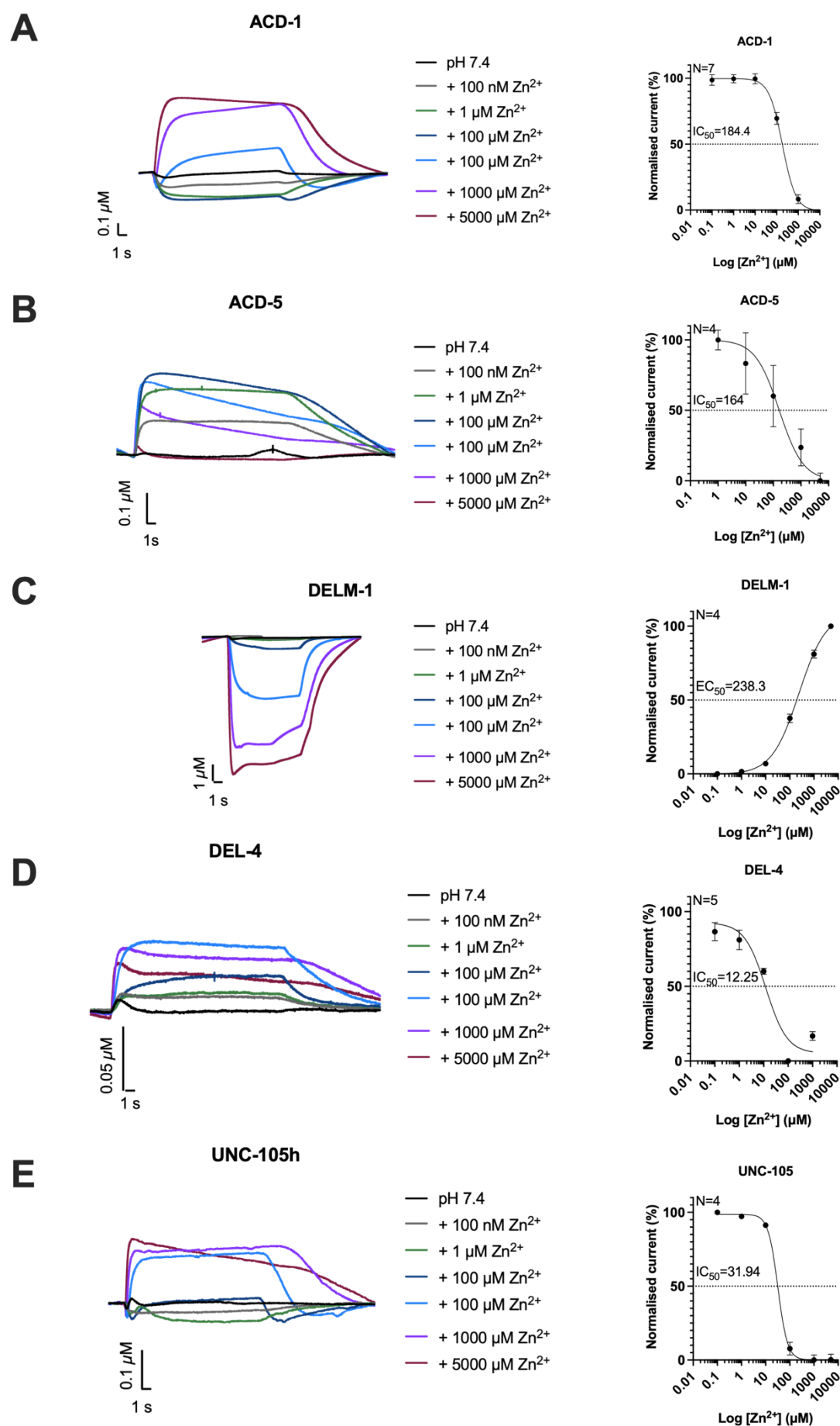
432

433   *Figure 9: Zinc modulation of acid-inhibited DEG/ENaC channels in Xenopus oocytes.*
434   (A-E) Zn^{2+} modulate homomeric ACD-1, ACD-5, DELM-1, DEL -4 and UNC-105 currents at pH 7.4 in a
435   dose-dependent manner. Shown are representative example traces (Left) and dose response curves
436   (Right) for each channel: Zn^{2+} dose-response of ACD-1 with an IC_{50} of 184.4 μM Zn^{2+}, ACD-5 with an
437   IC_{50} of 165 μM, DELM-1 with an EC_{50} of 238.3 μM, DEL-4 with an IC_{50} of 12.25 μM, and DEL-4 with an
438   IC_{50} of 31.94 μM Zn^{2+}. Baseline subtraction and drift correction was applied in the Roobocye2+
439   software. Currents were recorded at a holding potential of - 60mV and are normalised to the
440   maximum current (I_{max}) calculated for each oocyte individually, and best fitted with the Hill equation
441   (Variable slope). Error bars represent Mean ± SEM.
442

Acid-activated DEG/ENaCs are expressed in both neurons and muscles

444   *C. elegans* DEG/ENaC expression has been described in various tissues including muscle,

445   neurons, glia, and intestinal epithelia (Park & Horvitz, 1986a; Chalfie & Wolinsky, 1990;

446   Driscoll & Chalfie, 1991; Huang *et al.*, 1995; Take-Uchi *et al.*, 1998; Wang *et al.*, 2008; Wang

447   *et al.*, 2012; Han *et al.*, 2013). The previously-described acid-inhibited DEG/ENaCs are

448   expressed mainly in non-neuronal tissue with the exception of DEL-4 which is expressed in

449   neurons (Petratou *et al.*, submitted); ACD-1 and DELM-1 and DELM-2 are expressed in glia,

450   ACD-5 and FLR-1 in the intestine, and UNC-105 is expressed in the body-wall muscle (Park &

451   Horvitz, 1986a; Take-Uchi *et al.*, 1998; Wang *et al.*, 2008; Han *et al.*, 2013; Kaulich *et al.*, 2021).

452   To characterise the expression patterns of the acid-activated *C. elegans* DEG/ENaCs,

453   we used transcriptional reporters. We confirmed previous reports that the *asic-1* promoter

454   drives expression in the ADE, CEP, PVQ, PDE and PVD neurons (Voglis & Tavernarakis, 2008;

455   Husson *et al.*, 2012; De Stasio *et al.*, 2018) and also observed expression in FLP and ventral

456   cord neurons (Figure 10). The *acd-2* transcriptional reporter showed low-level expression in

457   unidentified anterior neurons or glia in the head. Our *del-9* reporter was expressed in anterior

458   and posterior body wall muscles, egg-laying muscles as well as head and tail neurons including

459   AVL and PVQ. These and previous results show that the *C. elegans* acid-sensing DEG/ENaCs

460   are not confined to a particular tissue but can be expressed in both neuronal and non-

461   neuronal tissues.

462

A Promoter fusion — DIC — Merged

Pasic-1 (3.5kb)::mKate2

B

Pacd-2 (3kb)::GFP
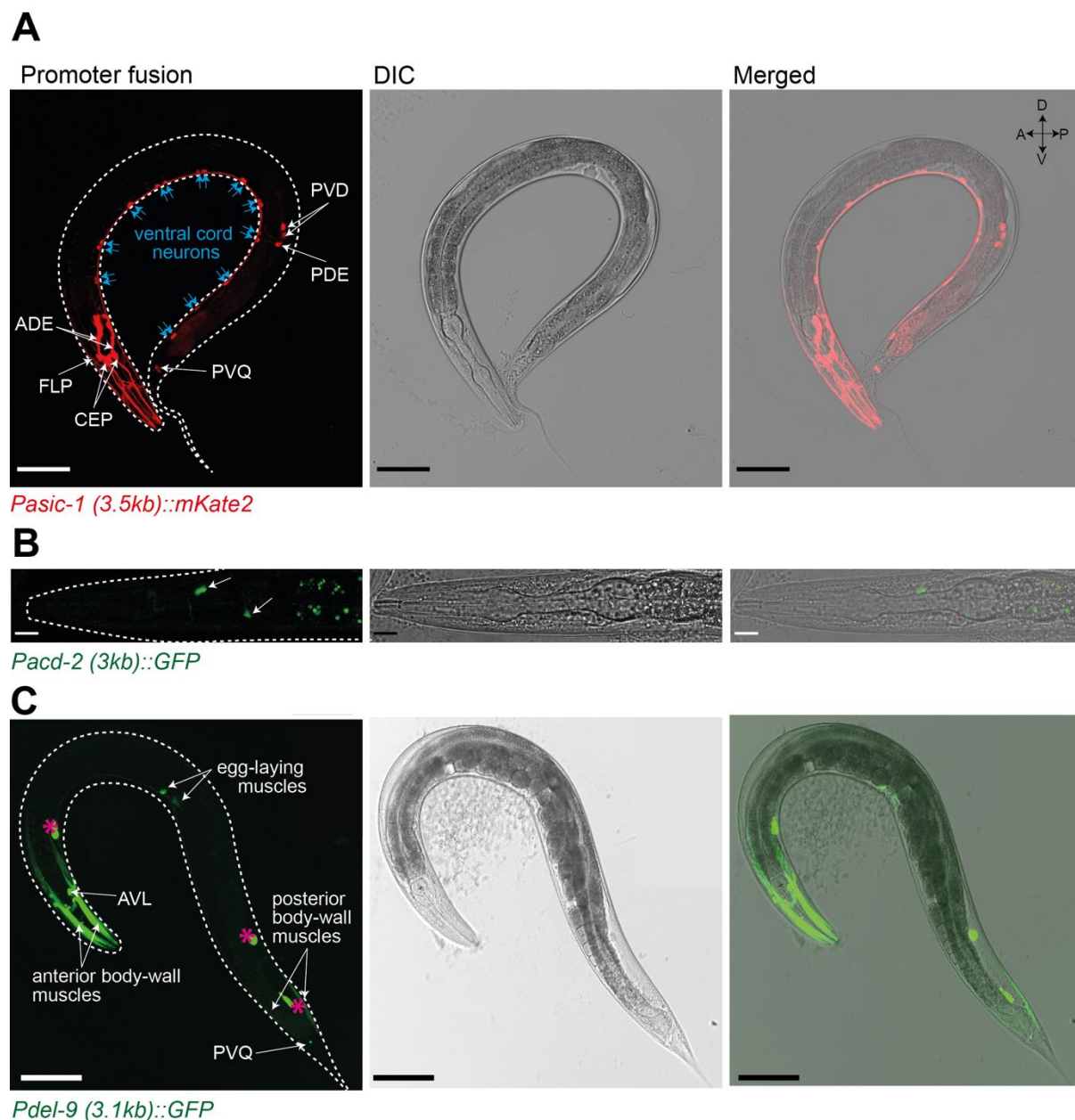
C

Pdel-9 (3.1kb)::GFP

Figure 10: *Acid-activated DEG/ENaCs are expressed in neuronal and non-neuronal tissue.*
Expression pattern of the transcriptional promoter fusions of the acid-activated DEG/ENaC genes with *mKate2* or *GFP* in L4 and young adults. (A) The *asic-1* promoter drives expression in the dopaminergic neurons and PVDs and FLPs. (B) *acd-2* promoter expression can be faintly detected in the head which based on localisation and RNA-sequencing data by (Cao *et al.*, 2017) could be neurons or glia cells. Green dots in the intestine are autofluorescence. (C) The *del-9* promoter drives expression in the body-wall and egg-laying muscles, in head neurons, PVQ neuron and the GABAergic neuron AVL. Pink asterisks indicate the coelomocytes (*Punc-122::GFP*, used as co-injection marker to select transgenic animals). Scale bars: (A) 100 µm (B) 10 µm (C) 100 µm.

Table 1: Summary of physiological properties of C. elegans acid-sensing DEG/ENaCs

		pH$_{50}$	Ion selectivity	Amiloride	Zn^{2+}	Expression	Reference
acid- inhibited	ACD-1	6.4	Na$^+$>Li$^+$>K$^+$	IC$_{50}$=99 µM	EC$_{50}$=184.4 µM	glia	(Wang *et al.*, 2008)
	ACD-5	4.87 (inhibitory) 6.48 (excitatory)	Li$^+$> K$^+$=Na$^+$	IC$_{50}$=131 µM	IC$_{50}$=164 µM	intestine	(Kaulich *et al.*, 2021)
	DEL-4	5.7	Na$^+$=Li$^+$>K$^+$	IC$_{50}$=179 µM	IC$_{50}$=12.25 µM	neurons	(Petratou *et al.*, submitted)
	DELM-1	5.75	Li$^+$>Na$^+$>K$^+$	IC$_{50}$=120 µM	EC$_{50}$=238.3 µM	glia	(Han *et al.*, 2013)
	UNC-105	6.42	Na$^+$=K$^+$	IC$_{50}$= 14.56 µM	IC$_{50}$=31.94 µM	muscle	(Garcia-Anoveros *et al.*, 1998; Jospin & Allard, 2004)
acid- activated	ACD-2	5.03	Li$^+$=Na$^+$>K$^+$	IC$_{50}$=84 µM	IC$_{50}$=46.39 µM	head neurons/glia	
	ASIC-1	4.49	K$^+$=Li$^+$>Na$^+$	IC$_{50}$=134 µM	IC$_{50}$=132.4 µM	neurons	
	DEL-9	4.27	Na$^+$=Li$^+$=K$^+$	*Acid-induced currents are insensitive*	IC$_{50}$=58.33 µM	muscle, neurons	

477 Table showing the channel properties described here, incorporated with those reported in the

478 referenced indicated.

479

Discussion

481 The acid-sensing members of the DEG/ENaCs, the ASICs, are proton receptors that can sense

482 changes in extracellular pH in neuronal and non-neuronal tissues. *C. elegans* is a genetic

483 model system that pioneered research into DEG/ENaCs, however, relatively little is known

484 about pH-sensing by *C. elegans* DEG/ENaCs or their modulation by other molecules. We have

485 shown here that there are at least three *C. elegans* acid-activated DEG/ENaCs, ASIC-1, ACD-2

486 and DEL-9. All three acid-activated channels are cation channels that are activated by

487 increasing proton concentrations and inhibited by the trace element zinc. ASIC-1 and ACD-2

488 can also be blocked by the anti-hypertensive drug amiloride in a dose-dependent manner.

24

489   Our findings raise the question of the channels' functional roles *in vivo*. In particular,
490   it is unclear whether these channels would encounter a prolonged acidic environment under
491   physiological conditions, especially as the acid-sensing DEG/ENaCs differ from the vertebrate
492   ASICs in that they do not desensitise during the course of the proton stimulation (whereas
493   the vertebrate ASICs do so within milliseconds). For instance, the murine ASIC1 is activated
494   by protonergic neurotransmission, which might constitute a short increase in acidification
495   due to neurotransmission, but could also represent a highly variable acidic environment
496   depending on the rate of exocytosis (Du et al., 2014). Protons are co-packed in presynaptic
497   vesicles with other neurotransmitters by the action of the proton pump Vacuolar-type ATPase
498   (V-ATPase) (Gowrisankaran & Milosevic, 2020), and then co-released into the synaptic cleft,
499   inducing a brief local drop in pH of 0.2 to 0.6 units (Miesenbock *et al.*, 1998; Du *et al.*, 2014;
500   Zeng *et al.*, 2015). This in turn stimulates postsynaptic receptors such as the ASICs (Soto *et al.*,
501   2018). Similarly, presynaptic vesicles of glutamatergic hippocampal neurons also co-release
502   millimolar concentrations of Zn^{2+} during synaptic transmission (Assaf & Chung, 1984; Howell
503   *et al.*, 1984; Frederickson & Moncrieff, 1994) which could in turn modulate ASIC channels
504   during neurotransmission.

505   A role in neurotransmission may also be relevant to the *in vivo* function of *C. elegans*
506   channels, in particular ASIC-1. We have shown that ASIC-1, like the murine ASIC1, can be
507   activated by external protons in a concentration-dependent manner, suggesting that, ASIC-1
508   is involved in synaptic transmission in a similar way. This would fit well with behavioural and
509   genetic evidence that it localizes to presynaptic terminals of dopaminergic neurons and
510   enhances dopamine release required for associative learning (Voglis & Tavernarakis, 2008).
511   Our electrophysiological characterisation of ASIC-1 *in vitro* supports the authors' proposed
512   working model in which ASIC-1 at the presynaptic terminal is activated by a local drop in pH
513   during the release of dopamine from the pre-synaptic terminal, and this activation of ASIC-1
514   then promotes sustained dopaminergic signalling (Voglis & Tavernarakis, 2008). Expression in
515   head neurons or glia suggests a likely role for ACD-2 in modulating synaptic function, similar
516   to that described for the *C. elegans* ASIC-1, or modulating neuronal function as described for
517   the glial DELM-1, DELM-2 or ACD-1 (Voglis & Tavernarakis, 2008; Wang *et al.*, 2008; Han *et*
518   *al.*, 2013). DEL-9 is expressed in the GABAergic motor neuron AVL, which synapses on to the
519   enteric muscle and regulates the expulsion step of the defecation motor program (McIntire
520   *et al.*, 1993), and the egg-laying muscles which are responsible for the expulsion of eggs. This

521 suggests that, in common with the acid-inhibited channels ACD-5 and FLR-1/ACD-3/DEL-5

522 (Kaulich *et al.*, 2021), it could function in the coordination of rhythmic behaviours.

523 We also expanded the characterisation of acid-inhibited channels, of which we

524 identified four further members, ACD-5, DELM-1, DEL-4 and UNC-105, in addition to the

525 previously described ACD-1 (Wang *et al.*, 2008). This shows that even on exposure to the same

526 stimulus (here protons), these channels show a remarkable diversity of functions, most likely

527 responding to the demands in their particular environment (i.e. in the intestinal lumen

528 (Kaulich *et al.*, 2021), duct of the kidney (Collier & Snyder, 2009), and the synaptic cleft (Du *et*

529 *al.*, 2014)). UNC-105 functions in the body wall muscle and mutations that increase Na$^+$ influx

530 cause hypercontraction indicating a role in maintaining cell excitability (Park & Horvitz, 1986b;

531 Garcia-Anoveros *et al.*, 1998). Previous research, involving electrophysiological recording

532 from muscle, has already suggested that *C. elegans* body muscles are proton-sensitive (Jospin

533 *et al.*, 2004): under voltage-clamp and current-clamp conditions, decreasing external pH from

534 7.2 to 6.1 led to a reversible depolarization of muscle cells (Jospin & Allard, 2004). However,

535 in an *unc-105* null mutant the pH-sensitive current could still be observed, and acid-evoked

536 depolarization is moreover suggestive of the involvement of an acid-activated, muscle-

537 expressed channel, such as DEL-9 rather than an acid-inhibited channel like UNC-105. The

538 roles of acid-sensing DEG/ENaCs in body muscle clearly merits further investigation.

539 Finally, DEG/ENaCs can also exert an effect on neuronal function from surrounding

540 glia. Mutation of the *C. elegans* DEG/ENaC, *acd-1,* expressed in the amphid socket cells,

541 exacerbates these sensory deficits, and deficits caused by mutations of genes implicated in

542 sensory functions in other amphid neurons (Wang *et al.*, 2008; Wang *et al.*, 2012). Artificially

543 increasing intracellular Ca^{2+} levels in one of these neurons bypassed the need for ACD-1,

544 supporting the idea that ACD-1 modulates neuronal excitability (Wang *et al.*, 2008; Wang *et*

545 *al.*, 2012). This idea is supported by the second example: DELM-1 (which we have shown is

546 acid-inhibited, like ACD-1) and DELM-2 are expressed in the glia cells associated with nose

547 touch neurons, the OLQs and IL1, on which they appear to exert a similar effect (Han *et al.*,

548 2013). Vertebrate ASICs are also expressed in glia and, for example, some of the roles

549 identified in learning may in fact be glia-based (Hill & Ben-Shahar, 2018), so disentangling glial

550 from neuronal functions represents an exciting avenue for future investigations. In summary,

551 *C. elegans* acid-sensitive ion channels appear to be involved in regulating the general

552 excitability of a wide range of cell types, including muscle, glia, epithelia and neurons, and in

553 a wide range of functional contexts. Precise channel localisation (for example, to identify

554 localisation at specific synapses), and correlation with behavioural testing, are the necessary

555 next steps for exploring *in vivo* function.

556   The expanded group of *C. elegans* DEG/ENaC thus encompasses a huge variety of

557 channel properties, with respect to proton-dependence profiles, their interactions with

558 amiloride, zinc and NSAIDs and mechanosensitivity (Chalfie & Sulston, 1981; Chatzigeorgiou

559 *et al.*, 2010; Geffeney *et al.*, 2011; Fechner *et al.*, 2021). These distinct functional capabilities

560 do not necessarily cluster with overall sequence similarity. For example, in our phylogram

561 (Figure 1), whereas ACD-1, ACD-5 and DELM-1 cluster closely to each other, the two other

562 acid-inhibited subunits, DEL-4 and UNC-105, are closer to ASIC-1 and the mechanosensitive

563 members, and none of the three acid-activated subunits cluster together. Disentangling the

564 molecular basis of this diversity of function, and comparison across phyla, represents an

565 important avenue for better understanding structure-function of the DEG/ENaCs. For

566 instance, solving the structure of the chicken ASIC1 N-terminus and sequence comparison

567 with other members revealed conserved residues important for ion-selectivity and gating

568 (Yoder & Gouaux, 2020). Likewise, correlating sequence disparities with differences in

569 function can play a key role in revealing their molecular basis.

570   Finally, our initial characterisation of these channels also provides a starting point for

571 compound screens against these ASICs for drug discovery, both *in vivo* in the worm and in

572 *Xenopus* oocytes, the former being particularly well-adapted to high throughput screening.

573 Anti-helminthic drugs act on ion channels found in neurons and muscles and our

574 characterisation has shown that *C. elegans* acid-activated DEG/ENaCs are present in both

575 tissues, making them a good potential avenue with which to target parasitic relatives.

576

577

References

Adams CM, Snyder PM & Welsh MJ. (1999). Paradoxical stimulation of a DEG/ENaC channel by amiloride. *J Biol Chem* **274,** 15500-15504.

Assaf SY & Chung SH. (1984). Release of endogenous Zn2+ from brain tissue during activity. *Nature* **308,** 734-736.

Awayda MS & Subramanyam M. (1998). Regulation of the epithelial Na+ channel by membrane tension. *J Gen Physiol* **112,** 97-111.

Baconguis I, Bohlen CJ, Goehring A, Julius D & Gouaux E. (2014). X-ray structure of acid-sensing ion channel 1-snake toxin complex reveals open state of a Na(+)-selective channel. *Cell* **156,** 717-729.

Baron A, Schaefer L, Lingueglia E, Champigny G & Lazdunski M. (2001). Zn2+ and H+ are coactivators of acid-sensing ion channels. *J Biol Chem* **276,** 35361-35367.

Bentley PJ. (1968). Amiloride: a potent inhibitor of sodium transport across the toad bladder. *J Physiol* **195,** 317-330.

Besson T, Lingueglia E & Salinas M. (2017). Pharmacological modulation of Acid-Sensing Ion Channels 1a and 3 by amiloride and 2-guanidine-4-methylquinazoline (GMQ). *Neuropharmacology* **125,** 429-440.

Bhagatwala J, Harris RA, Parikh SJ, Zhu H, Huang Y, Kotak I, Seigler N, Pierce GL, Egan BM & Dong Y. (2014). Epithelial sodium channel inhibition by amiloride on blood pressure and cardiovascular disease risk in young prehypertensives. *J Clin Hypertens (Greenwich)* **16,** 47-53.

Bianchi L, Gerstbrein B, Frokjaer-Jensen C, Royal DC, Mukherjee G, Royal MA, Xue J, Schafer WR & Driscoll M. (2004). The neurotoxic MEC-4(d) DEG/ENaC sodium channel conducts calcium: implications for necrosis initiation. *Nat Neurosci* **7,** 1337-1344.

Boiko N, Kucher V, Stockand JD & Eaton BA. (2012). Pickpocket1 Is an Ionotropic Molecular Sensory Transducer. *J Biol Chem* **287,** 39878–39886.

Canessa CM, Horisberger JD & Rossier BC. (1993). Epithelial sodium channel related to proteins involved in neurodegeneration. *Nature* **361,** 467-470.

Canessa CM, Schild L, Buell G, Thorens B, Gautschi I, Horisberger JD & Rossier BC. (1994). Amiloride-sensitive epithelial Na+ channel is made of three homologous subunits. *Nature* **367,** 463-467.

Cao J, Packer JS, Ramani V, Cusanovich DA, Huynh C, Daza R, Qiu X, Lee C, Furlan SN, Steemers FJ, Adey A, Waterston RH, Trapnell C & Shendure J. (2017). Comprehensive single-cell transcriptional profiling of a multicellular organism. *Science* **357,** 661-667.

640   Carattino MD & Della Vecchia MC. (2012). Contribution of residues in second
641   transmembrane domain of ASIC1a protein to ion selectivity. *J Biol Chem* **287,** 12927-
642   12934.

644   Chalfie M & Sulston J. (1981). Developmental genetics of the mechanosensory neurons of
645   Caenorhabditis elegans. *Dev Biol* **82,** 358-370.

647   Chalfie M & Wolinsky E. (1990). The identification and suppression of inherited
648   neurodegeneration in Caenorhabditis elegans. *Nature* **345,** 410-416.

650   Chatzigeorgiou M, Grundy L, Kindt KS, Lee WH, Driscoll M & Schafer WR. (2010). Spatial
651   asymmetry in the mechanosensory phenotypes of the C. elegans DEG/ENaC gene
652   mec-10. *Journal of neurophysiology* **104,** 3334-3344.

654   Chen J, Winarski KL, Myerburg MM, Pitt BR & Sheng S. (2012). Probing the structural basis of
655   Zn^{2+} regulation of the epithelial Na^+ channel. *J Biol Chem* **287,** 35589-35598.

657   Chen X, Polleichtner G, Kadurin I & Grunder S. (2007). Zebrafish acid-sensing ion channel
658   (ASIC) 4, characterization of homo- and heteromeric channels, and identification of
659   regions important for activation by H^+. *J Biol Chem* **282,** 30406-30413.

661   Ciccarelli FD, Doerks T, von Mering C, Creevey CJ, Snel B & Bork P. (2006). Toward automatic
662   reconstruction of a highly resolved tree of life. *Science* **311,** 1283-1287.

664   Collier DM & Snyder PM. (2009). Extracellular protons regulate human ENaC by modulating
665   Na^+ self-inhibition. *J Biol Chem* **284,** 792-798.

667   De Stasio EA, Mueller KP, Bauer RJ, Hurlburt AJ, Bice SA, Scholtz SL, Phirke P, Sugiaman-
668   Trapman D, Stinson LA, Olson HB, Vogel SL, Ek-Vazquez Z, Esemen Y, Korzynski J,
669   Wolfe K, Arbuckle BN, Zhang H, Lombard-Knapp G, Piasecki BP & Swoboda P. (2018).
670   An Expanded Role for the RFX Transcription Factor DAF-19, with Dual Functions in
671   Ciliated and Nonciliated Neurons. *Genetics* **208,** 1083-1097.

673   Driscoll M & Chalfie M. (1991). The mec-4 gene is a member of a family of Caenorhabditis
674   elegans genes that can mutate to induce neuronal degeneration. *Nature* **349,** 588-
675   593.

677   Du J, Reznikov LR, Price MP, Zha XM, Lu Y, Moninger TO, Wemmie JA & Welsh MJ. (2014).
678   Protons are a neurotransmitter that regulates synaptic plasticity in the lateral
679   amygdala. *Proc Natl Acad Sci U S A* **111,** 8961-8966.

681   Dulai JS, Smith ESJ & Rahman T. (2021). Acid-sensing ion channel 3: An analgesic target.
682   *Channels (Austin)* **15,** 94-127.

684   Elkhatib W, Smith CL & Senatore A. (2019). A $Na(+)$ leak channel cloned from Trichoplax
685   adhaerens extends extracellular pH and $Ca(2+)$ sensing for the DEG/ENaC family
686   close to the base of Metazoa. *J Biol Chem* **294,** 16320-16336.

687

688 Fazia T, Pastorino R, Notartomaso S, Busceti C, Imbriglio T, Cannella M, Gentilini D, Morani
689   G, Ticca A, Bitti P, Berzuini C, Dalmay T, Battaglia G & Bernardinelli L. (2019). Acid
690   sensing ion channel 2: A new potential player in the pathophysiology of multiple
691   sclerosis. *Eur J Neurosci* **49,** 1233-1243.
692

693 Fechner S, D'Alessandro I, Wang L, Tower C, Tao L & Goodman MB. (2021). DEG/ENaC/ASIC
694   channels vary in their sensitivity to anti-hypertensive and non-steroidal anti-
695   inflammatory drugs. *J Gen Physiol* **153**.
696

697 Frederickson CJ & Moncrieff DW. (1994). Zinc-containing neurons. *Biol Signals* **3,** 127-139.
698

699 Friese MA, Craner MJ, Etzensperger R, Vergo S, Wemmie JA, Welsh MJ, Vincent A & Fugger
700   L. (2007). Acid-sensing ion channel-1 contributes to axonal degeneration in
701   autoimmune inflammation of the central nervous system. *Nat Med* **13,** 1483-1489.
702

703 Garcia-Anoveros J, Garcia JA, Liu JD & Corey DP. (1998). The nematode degenerin UNC-105
704   forms ion channels that are activated by degeneration- or hypercontraction-causing
705   mutations. *Neuron* **20,** 1231-1241.
706

707 Geffeney SL, Cueva JG, Glauser DA, Doll JC, Lee TH, Montoya M, Karania S, Garakani AM,
708   Pruitt BL & Goodman MB. (2011). DEG/ENaC but not TRP channels are the major
709   mechanoelectrical transduction channels in a C. elegans nociceptor. *Neuron* **71,** 845-
710   857.
711

712 Gerlt JA. (2017). Genomic Enzymology: Web Tools for Leveraging Protein Family Sequence-
713   Function Space and Genome Context to Discover Novel Functions. *Biochemistry* **56,**
714   4293-4308.
715

716 Gerlt JA, Bouvier JT, Davidson DB, Imker HJ, Sadkhin B, Slater DR & Whalen KL. (2015).
717   Enzyme Function Initiative-Enzyme Similarity Tool (EFI-EST): A web tool for
718   generating protein sequence similarity networks. *Biochim Biophys Acta* **1854,** 1019-
719   1037.
720

721 Gowrisankaran S & Milosevic I. (2020). Regulation of synaptic vesicle acidification at the
722   neuronal synapse. *IUBMB Life* **72,** 568-576.
723

724 Han L, Wang Y, Sangaletti R, D'Urso G, Lu Y, Shaham S & Bianchi L. (2013). Two novel
725   DEG/ENaC channel subunits expressed in glia are needed for nose-touch sensitivity
726   in Caenorhabditis elegans. *J Neurosci* **33,** 936-949.
727

728 Hardege I, Xu S, Gordon RD, Thompson AJ, Figg N, Stowasser M, Murrell-Lagnado R &
729   O'Shaughnessy KM. (2015). Novel Insertion Mutation in KCNJ5 Channel Produces
730   Constitutive Aldosterone Release From H295R Cells. *Mol Endocrinol* **29,** 1522-1530.
731

732 Hill AS & Ben-Shahar Y. (2018). The synaptic action of Degenerin/Epithelial sodium channels.
733   *Channels (Austin, Tex)* **12,** 262-275.

734

735 Howell GA, Welch MG & Frederickson CJ. (1984). Stimulation-induced uptake and release of
736   zinc in hippocampal slices. *Nature* **308,** 736-738.

737

738 Huang M, Gu G, Ferguson EL & Chalfie M. (1995). A stomatin-like protein necessary for
739   mechanosensation in C. elegans. *Nature* **378,** 292-295.

740

741 Husson SJ, Costa WS, Wabnig S, Stirman JN, Watson JD, Spencer WC, Akerboom J, Looger LL,
742   Treinin M, Miller DM, 3rd, Lu H & Gottschalk A. (2012). Optogenetic analysis of a
743   nociceptor neuron and network reveals ion channels acting downstream of primary
744   sensors. *Curr Biol* **22,** 743-752.

745

746 Jiang Q, Zha XM & Chu XP. (2012). Inhibition of human acid-sensing ion channel 1b by zinc.
747   *Int J Physiol Pathophysiol Pharmacol* **4,** 84-93.

748

749 Jospin M & Allard B. (2004). An amiloride-sensitive H+-gated Na+ channel in Caenorhabditis
750   elegans body wall muscle cells. *J Physiol* **559,** 715-720.

751

752 Jospin M, Mariol MC, Segalat L & Allard B. (2004). Patch clamp study of the UNC-105
753   degenerin and its interaction with the LET-2 collagen in Caenorhabditis elegans
754   muscle. *The Journal of physiology* **557,** 379-388.

755

756 Kaminski J, Gibson MK, Franzosa EA, Segata N, Dantas G & Huttenhower C. (2015). High-
757   Specificity Targeted Functional Profiling in Microbial Communities with ShortBRED.
758   *PLoS computational biology* **11,** e1004557-e1004557.

759

760 Katoh K, Misawa K, Kuma K & Miyata T. (2002). MAFFT: a novel method for rapid multiple
761   sequence alignment based on fast Fourier transform. *Nucleic Acids Res* **30,** 3059-
762   3066.

763

764 Katoh K & Standley DM. (2013). MAFFT multiple sequence alignment software version 7:
765   improvements in performance and usability. *Mol Biol Evol* **30,** 772-780.

766

767 Kaulich E, Ackley BD, Tang Y, Hardege I, Schafer WR & Walker DS. (2021). Distinct roles for
768   two Caenorhabditis elegans acid-sensing ion channels in an ultradian clock. *bioRxiv*.

769

770 Keiser J & Utzinger J. (2008). Efficacy of current drugs against soil-transmitted helminth
771   infections: systematic review and meta-analysis. *JAMA* **299,** 1937-1948.

772

773 Kellenberger S, Gautschi I & Schild L. (2003). Mutations in the epithelial Na+ channel ENaC
774   outer pore disrupt amiloride block by increasing its dissociation rate. *Mol Pharmacol*
775   **64,** 848-856.

776

777 Kuraku S, Zmasek CM, Nishimura O & Katoh K. (2013). aLeaves facilitates on-demand
778   exploration of metazoan gene family trees on MAFFT sequence alignment server
779   with enhanced interactivity. *Nucleic Acids Res* **41,** W22-28.

780

781 Larkin MA, Blackshields G, Brown NP, Chenna R, McGettigan PA, McWilliam H, Valentin F,
782   Wallace IM, Wilm A, Lopez R, Thompson JD, Gibson TJ & Higgins DG. (2007). Clustal
783   W and Clustal X version 2.0. *Bioinformatics* **23,** 2947-2948.
784

785 Letunic I & Bork P. (2019). Interactive Tree Of Life (iTOL) v4: recent updates and new
786   developments. *Nucleic Acids Res* **47,** W256-W259.
787

788 Levin BJ, Huang YY, Peck SC, Wei Y, Martínez-Del Campo A, Marks JA, Franzosa EA,
789   Huttenhower C & Balskus EP. (2017). A prominent glycyl radical enzyme in human
790   gut microbiomes metabolizes trans-4-hydroxy-l-proline. *Science (New York, NY)* **355**.
791

792 Li T, Yang Y & Canessa CM. (2009). Interaction of the aromatics Tyr-72/Trp-288 in the
793   interface of the extracellular and transmembrane domains is essential for proton
794   gating of acid-sensing ion channels. *J Biol Chem* **284,** 4689-4694.
795

796 Li WG, Yu Y, Huang C, Cao H & Xu TL. (2011). Nonproton ligand sensing domain is required
797   for paradoxical stimulation of acid-sensing ion channel 3 (ASIC3) channels by
798   amiloride. *J Biol Chem* **286,** 42635-42646.
799

800 Loytynoja A & Goldman N. (2010). webPRANK: a phylogeny-aware multiple sequence aligner
801   with interactive alignment browser. *BMC Bioinformatics* **11,** 579.
802

803 Matasic DS, Holland N, Gautam M, Gibbons DD, Kusama N, Harding AMS, Shah VS, Snyder
804   PM & Benson CJ. (2021). Paradoxical Potentiation of Acid-Sensing Ion Channel 3
805   (ASIC3) by Amiloride via Multiple Mechanisms and Sites Within the Channel. *Front
806   Physiol* **12,** 750696.
807

808 McIntire SL, Jorgensen E, Kaplan J & Horvitz HR. (1993). The GABAergic nervous system of
809   Caenorhabditis elegans. *Nature* **364,** 337-341.
810

811 Miesenbock G, De Angelis DA & Rothman JE. (1998). Visualizing secretion and synaptic
812   transmission with pH-sensitive green fluorescent proteins. *Nature* **394,** 192-195.
813

814 O'Brodovich H, Canessa C, Ueda J, Rafii B, Rossier BC & Edelson J. (1993). Expression of the
815   epithelial Na+ channel in the developing rat lung. *Am J Physiol* **265,** C491-496.
816

817 Ortega-Ramirez A, Vega R & Soto E. (2017). Acid-Sensing Ion Channels as Potential
818   Therapeutic Targets in Neurodegeneration and Neuroinflammation. *Mediators
819   Inflamm* **2017,** 3728096.
820

821 Palmer LG & Frindt G. (1986). Amiloride-sensitive Na channels from the apical membrane of
822   the rat cortical collecting tubule. *Proc Natl Acad Sci U S A* **83,** 2767-2770.
823

824 Park EC & Horvitz HR. (1986a). C. elegans unc-105 mutations affect muscle and are
825   suppressed by other mutations that affect muscle. *Genetics* **113,** 853-867.
826

827 Park EC & Horvitz HR. (1986b). Mutations with dominant effects on the behavior and
828   morphology of the nematode Caenorhabditis elegans. *Genetics* **113,** 821-852.
829

830 Paukert M, Babini E, Pusch M & Grunder S. (2004). Identification of the Ca2+ blocking site of
831   acid-sensing ion channel (ASIC) 1: implications for channel gating. *J Gen Physiol* **124,**
832   383-394.
833

834 Schild L, Schneeberger E, Gautschi I & Firsov D. (1997). Identification of amino acid residues
835   in the alpha, beta, and gamma subunits of the epithelial sodium channel (ENaC)
836   involved in amiloride block and ion permeation. *J Gen Physiol* **109,** 15-26.
837

838 Schneider CA, Rasband WS & Eliceiri KW. (2012). NIH Image to ImageJ: 25 years of image
839   analysis. *Nat Methods* **9,** 671-675.
840

841 Shannon P, Markiel A, Ozier O, Baliga NS, Wang JT, Ramage D, Amin N, Schwikowski B &
842   Ideker T. (2003). Cytoscape: a software environment for integrated models of
843   biomolecular interaction networks. *Genome Res* **13,** 2498-2504.
844

845 Soto E, Ortega-Ramirez A & Vega R. (2018). Protons as Messengers of Intercellular
846   Communication in the Nervous System. *Front Cell Neurosci* **12**.
847

848 Take-Uchi M, Kawakami M, Ishihara T, Amano T, Kondo K & Katsura I. (1998). An ion channel
849   of the degenerin/epithelial sodium channel superfamily controls the defecation
850   rhythm in Caenorhabditis elegans. *Proc Natl Acad Sci U S A* **95,** 11775-11780.
851

852 Tan G, Muffato M, Ledergerber C, Herrero J, Goldman N, Gil M & Dessimoz C. (2015).
853   Current Methods for Automated Filtering of Multiple Sequence Alignments
854   Frequently Worsen Single-Gene Phylogenetic Inference. *Syst Biol* **64,** 778-791.
855

856 Teiwes J & Toto RD. (2007). Epithelial sodium channel inhibition in cardiovascular disease. A
857   potential role for amiloride. *Am J Hypertens* **20,** 109-117.
858

859 Vina E, Parisi V, Cabo R, Laura R, Lopez-Velasco S, Lopez-Muniz A, Garcia-Suarez O, Germana
860   A & Vega JA. (2013). Acid-sensing ion channels (ASICs) in the taste buds of adult
861   zebrafish. *Neurosci Lett* **536,** 35-40.
862

863 Voglis G & Tavernarakis N. (2008). A synaptic DEG/ENaC ion channel mediates learning in C.
864   elegans by facilitating dopamine signalling. *EMBO J* **27,** 3288-3299.
865

866 Voilley N. (2004). Acid-sensing ion channels (ASICs): new targets for the analgesic effects of
867   non-steroid anti-inflammatory drugs (NSAIDs). *Curr Drug Targets Inflamm Allergy* **3,**
868   71-79.
869

870 Voilley N, de Weille J, Mamet J & Lazdunski M. (2001). Nonsteroid Anti-Inflammatory Drugs
871   Inhibit Both the Activity and the Inflammation-Induced Expression of Acid-Sensing
872   Ion Channels in Nociceptors. *J Neurosci* **21,** 8026–8033.
873

874   Vullo S & Kellenberger S. (2020). A molecular view of the function and pharmacology of
875   acid-sensing ion channels. *Pharmacol Res* **154,** 104166.
876

877   Waldmann R, Champigny G, Bassilana F, Heurteaux C & Lazdunski M. (1997). A proton-gated
878   cation channel involved in acid-sensing. *Nature* **386,** 173-177.
879

880   Waldmann R, Champigny G, Voilley N, Lauritzen I & Lazdunski M. (1996). The mammalian
881   degenerin MDEG, an amiloride-sensitive cation channel activated by mutations
882   causing neurodegeneration in Caenorhabditis elegans. *The Journal of biological*
883   *chemistry* **271,** 10433-10436.
884

885   Wang Y, Apicella A, Jr., Lee SK, Ezcurra M, Slone RD, Goldmit M, Schafer WR, Shaham S,
886   Driscoll M & Bianchi L. (2008). A glial DEG/ENaC channel functions with neuronal
887   channel DEG-1 to mediate specific sensory functions in C. elegans. *EMBO J* **27,** 2388-
888   2399.
889

890   Wang Y, D'Urso G & Bianchi L. (2012). Knockout of glial channel ACD-1 exacerbates sensory
891   deficits in a C. elegans mutant by regulating calcium levels of sensory neurons. *J*
892   *Neurophysiol* **107,** 148-158.
893

894   Wang Y, Matthewman C, Han L, Miller T, Miller DM, 3rd & Bianchi L. (2013). Neurotoxic unc-
895   8 mutants encode constitutively active DEG/ENaC channels that are blocked by
896   divalent cations. *J Gen Physiol* **142,** 157-169.
897

898   Wiemuth D & Grunder S. (2010). A single amino acid tunes Ca2+ inhibition of brain liver
899   intestine Na+ channel (BLINaC). *J Biol Chem* **285,** 30404-30410.
900

901   Williamson SM, Robertson AP, Brown L, Williams T, Woods DJ, Martin RJ, Sattelle DB &
902   Wolstenholme AJ. (2009). The nicotinic acetylcholine receptors of the parasitic
903   nematode Ascaris suum: formation of two distinct drug targets by varying the
904   relative expression levels of two subunits. *PLoS Pathog* **5,** e1000517.
905

906   Wolstenholme AJ & Rogers AT. (2005). Glutamate-gated chloride channels and the mode of
907   action of the avermectin/milbemycin anthelmintics. *Parasitology* **131 Suppl,** S85-95.
908

909   Yoder N & Gouaux E. (2020). The His-Gly motif of acid-sensing ion channels resides in a
910   reentrant 'loop' implicated in gating and ion selectivity. *Elife* **9**.
911

912   Zallot R, Oberg N & Gerlt JA. (2019). The EFI Web Resource for Genomic Enzymology Tools:
913   Leveraging Protein, Genome, and Metagenome Databases to Discover Novel
914   Enzymes and Metabolic Pathways. *Biochemistry* **58,** 4169-4182.
915

916   Zallot R, Oberg NO & Gerlt JA. (2018). 'Democratized' genomic enzymology web tools for
917   functional assignment. *Curr Opin Chem Biol* **47,** 77-85.
918

919   Zeng WZ, Liu DS, Liu L, She L, Wu LJ & Xu TL. (2015). Activation of acid-sensing ion channels
920   by localized proton transient reveals their role in proton signaling. *Sci Rep* **5,** 14125.

921

922   Zhang P & Canessa CM. (2002). Single channel properties of rat acid-sensitive ion channel-
923   1alpha, -2a, and -3 expressed in Xenopus oocytes. *J Gen Physiol* **120,** 553-566.

924

925